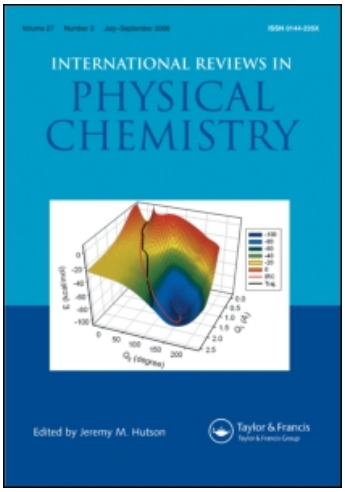


**International Reviews in Physical Chemistry**
Publication details, including instructions for authors and subscription information:
http://www.informaworld.com/smpp/title~content=t713724383

# Structural, photophysical and lasing properties of pyrromethene dyes

F. López Arbeloa[a]; J. Bañuelos[a]; V. Martínez[a]; T. Arbeloa[a]; I. López Arbeloa[a]
[a] Departamento Química Física, Universidad País Vasco-EHU, Apartado 644, 48080-Bilbao, Spain

**To cite this Article** Arbeloa, F. López , Bañuelos, J. , Martínez, V. , Arbeloa, T. and Arbeloa, I. López(2005) 'Structural, photophysical and lasing properties of pyrromethene dyes', International Reviews in Physical Chemistry, 24: 2, 339 — 374
**To link to this Article: DOI:** 10.1080/01442350500270551
**URL:** http://dx.doi.org/10.1080/01442350500270551

*International Reviews in Physical Chemistry*,
Vol. 24, No. 2, April–June 2005, 339–374

Taylor & Francis
Taylor & Francis Group

# Structural, photophysical and lasing properties of pyrromethene dyes

F. LÓPEZ ARBELOA*, J. BAÑUELOS, V. MARTÍNEZ,
T. ARBELOA and I. LÓPEZ ARBELOA

Departamento Química Física, Universidad País Vasco-EHU, Apartado 644,
48080-Bilbao, Spain

(*Received 12 April 2005; in final form 22 July 2005*)



The molecular structure and the photophysical properties of pyrromethene-$BF_2$ (PM) dyes are studied with the aim of finding the best structural and environmental conditions which optimize the laser performance of these dyes. To this end, UV–Vis absorption and fluorescence spectra and fluorescence decay curves of several PM dyes are registered in a multitude of solvents with different physicochemical properties and in polymeric solid matrices. Quantum mechanical calculations at different levels are also applied in order to explain the photophysical behaviour of these dyes. The studied pyrromethenes incorporate alkyl (methyl, ethyl and *tert*-butyl), sulfonate, cyano, and acetoxy- and methacryloyloxy-polymethylene groups in different positions of the chromophore. In the last case, the presence of the polymerizable acryloyl group facilitates the covalent linkage of the chromophore to a polymeric chain, of special technological interest in the development of tunable dye lasers in the solid state. From the experimental results and the theoretical calculations, we discuss different mechanisms of internal conversion for PM dyes, such as the loss in the planarity of the chromophore, the electron flow through the delocalized $\pi$-system, the vibrational coupling and the formation of an intramolecular charge transfer state. The present work demonstrates the good correlation between the photophysical and the lasing properties of PM dyes with different structural (substituents) and environmental (solvents and polymers) conditions.

## Contents



*Corresponding author. Email: fernando.lopezarbeloa@ehu.es

*International Reviews in Physical Chemistry*
ISSN 0144–235X print/ISSN 1366–591X online 
http://www.tandf.co.uk/journals
DOI: 10.1080/01442350500270551

## 1. Introduction

The study of the photophysics of organic dyes has received great technological interest because of their use as the active media in tunable lasers and in the development of photoelectronic devices [1–6]. Moreover, laser dyes have wide applications not only in photonics, but also as fluorescent probes, as molecular sensors, in light harvesting arrays and in information storage, among other uses [7–10]. Therefore the study of the photophysical properties of laser dyes is an important tool for the improvement of their photonic, photoelectronic and photosensor applications.

There are several commercially available laser-dye families covering the spectral region from UV to near-IR [11, 12]. They can be pumped with a wide variety of excitation sources, can emit in pulsed and continuous-wave forms and, owing to their wide gain band, can supply ultrashort pulses in the femtosecond timescale and can be tuned over a certain spectral range. These properties provide special applications of dye lasers in different fields, such as spectroscopy, optics, medicine, telecommunications, etc. [13, 14]. A chromophoric system must fulfil certain characteristics to be considered a laser dye:

- Strong absorption bands, enhancing the population inversion during the pumping process.
- Low probability of non-radiative deactivation processes from the emissive excited state, reducing the losses in the resonator cavity. The intersystem crossing probability is of special interest, since it can quench the emission from the fluorescent excited state and mainly populates the long-lifetime lowest triplet state ($T_1$). The triplet–triplet (T–T) absorption band, which can overlap with the lasing gain band, and the accumulation of molecules in the $T_1$ state, can strongly reduce the lasing efficiency [15].
- Large Stokes shifts and low tendency of the dye to self-aggregate. In order to guarantee high efficiency in the pumping process, the active media of tunable lasers require high optical density samples. In these conditions, the

dye aggregation can reduce the gain of the laser signal, since aggregates do not usually emit and are efficient quenchers of the fluorescence emission of monomers [16]. Moreover, the overlap between the absorption and fluorescence bands (governed by the Stokes shift) can increase the losses in the resonator cavity by the inner filter (i.e. the reabsorption effects) [17, 18].
- High thermo- and photostability of the dye, enhancing the operative time of the active media.

The scientific community is interested in the development of new active media for tunable lasers. Special efforts are oriented to improve the efficiency and the operative time of laser dyes. The synthesis of new active media can be focused in different ways [1]:

- The modification of the molecular structure of the chromophore system with adequate substituents to ameliorate the photophysical and lasing characteristics of well-known laser dyes [19].
- The incorporation of the dyes in host materials. Usually, the active media are liquid solutions of the dye; however, the introduction of the dye in solid matrices could design dye lasers in the solid state [20–24]. The development of solid state tunable lasers would imply important technological advantages with respect to the present commercial dye lasers, such as better manageability, versatility and miniaturization of the laser experimental set up, besides the lack of toxic and flammable solvents [25]. The most-used solid host matrices for laser dyes are organic polymers and sol–gel inorganic crystals. Organic polymers provide good optical homogeneity and excellent compatibility with the organic dye, for instance, the structure and chemical composition of the host materials can be easily modified to accommodate the organic guest molecules [21, 23]. The development of the sol–gel technique at room temperature has allowed the incorporation of organic dyes in inorganic matrices, leading to guest–host materials with good thermal properties and high radiation damage threshold [26].
- The synthesis of new dye families. In this sense, Boyer and coworkers synthesized new laser dyes, called boron-dipyrromethenes or pyrromethene-$BF_2$ complexes (PM), by the fluoroboration of two pyrrole units linked by a methylene group [27, 28]. These dyes present strong absorption and fluorescence bands in the green–red part of the visible region, giving rise to high florescence quantum yields and lasing efficiencies [29–37]. Moreover, due to their low probability of T–T absorption (estimated to be one-fifth of that of rhodamines), they provide better lasing performance than rhodamines, the most-used dyes as active media in tunable lasers [38, 39]. On the other hand, PM dyes generally present higher photostability than rhodamine dyes [40–42].

While the laser characteristics of PM dyes have been profoundly studied in the last few years [22, 24, 43, 44], their photophysical properties have not been so extensively studied. The aim of this work is to summarize the photophysical information of PM dyes as well as to analyse the influence of several structural and environmental factors on their photophysics. This knowledge is essential to predict the best conditions

to optimize the lasing efficiency of these dyes, since a satisfactory correlation between the photophysical properties (fluorescence wavelength and quantum yield) and lasing characteristics (laser wavelength and efficiency) has been established [45, 46]. Moreover, the understanding of the photophysical behaviour of PM dyes should be of interest in the design of new molecular sensors and fluorescent probes.

The photophysical properties of PMs are now overviewed, where several factors, such as the type and the position of the substituents, the nature of the solvent and the incorporation in polymeric solid matrices (both as dopant or covalently bound to the polymeric chain), are discussed. These photophysical properties are correlated with their laser characteristics, recorded by the Costela and Garcia research group [21, 23, 24]. Different commercial PM dyes (scheme 1) have been studied in several solvents, including apolar, polar/aprotic and polar/protic media. The photophysics of PM567 dye ($R_1 = C_2H_5$ and $R_2 = CH_3$), probably the most-used PM dye, is also analysed in polymethyl methacrylate (PMMA) matrices with different cross-linking agents [47]. On the other hand, analogues of the PM567 dye, with a polymerizable methacryloyloxy end group, have been used in order to covalently incorporate PM dyes to polymeric chains [48, 49].

The experimental results are discussed on the basis of theoretical quantum mechanical calculations. For this purpose, several calculation methods at the semiempirical, *ab initio* and the density functional theory (DFT) levels have been applied. The theoretical calculations are oriented to provide the optimized geometry, the electronic density distribution and the absorption and fluorescence characteristics of the dye in the gas phase and in solution, considering different models of solvation.



## 2. Methodology

### 2.1. *Dyes*

All the studied 4,4-difluoro-4-bora-3a,4a-diaza-*s*-indacene dyes presented methyl groups at the 1, 3, 5 and 7 positions and differ in the substitution at the 2, 6 and 8 positions. The commercial PM dyes (supplied by Exciton, laser grade) had alkyl groups: methyl (PM546) at the 8 position, ethyl (PM567), *tert*-butyl (PM597) or sulfonate (PM556) groups at the 2 and 6 positions, and acetoxymethylene (PM605) or cyano (PM650) group at the 8 position (see the molecular structures in scheme 1).

With the aim of covalently binding the chromophore to the polymeric chain, a series of analogues of the PM567 was synthesized by Amat and cowokers [48] by the

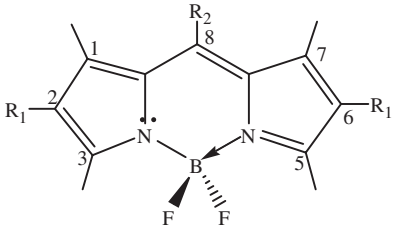


| Dye | $R_1$ | $R_2$ |
|---|---|---|
| PM546 | H | $CH_3$ |
| PM556 | $SO_3^-Na^+$ | $CH_3$ |
| PM567 | $C_2H_5$ | $CH_3$ |
| PM597 | $C(CH_3)_3$ | $CH_3$ |
| PM605 | $C_2H_5$ | $CH_2OCOCH_3$ |
| PM650 | $CH_3$ | CN |

Scheme 1. Molecular structures of commercial PM dyes.

introduction of a polymerizable methacryloyloxy group at the 8 position separated from the chromophore by a polymethylene chain with different lengths (PXMA with X = 1, 3, 5, 10 or 15, scheme 2). In order to understand the influence of the linking chain in the photophysics of the PM chromophore, the corresponding analogues with an acetoxy group (PXAc) were also previously obtained (scheme 2) [48].

A phenyl group was also included in position 8 as a spacer between the methacryloyloxy or acetoxy groups (PArXMA and PArXAc) and the chromophore (scheme 2) [49]. The phenyl group is *para*-substituted by a chain with one or three methylene units. The double linkage was also considered through the 2 and 6 positions, where the two methacryloyloxy groups with three methylene units, and their corresponding acetoxy models, have been incorporated (scheme 2).

The photophysical properties of the commercial PMs and the aromatic PAr1Ac analogue are studied in a wide variety of solvents, taking into account apolar (hydrocarbons), polar (ethers, ketones, esters, amides, ...) and polar/protic (alcohols) media. All the solvents were of spectroscopic grade (Merck, Fluka or Aldrich) and employed without further purification. The photophysics of the rest of the PM analogues were registered in six representative solvents from apolar (*c*-hexane) to polar (acetone and ethyl acetate) and protic (ethanol, methanol and trifluoroethanol) media.

The intrinsic photophysical properties of PM dyes were registered in diluted solutions ($2 \times 10^{-6}$ M) using a 1 cm optical pathway quartz cuvette. The solutions in the different solvents were prepared by taking the appropriate volume of a concentrated stock solution of each dye in acetone and, after vacuum evaporation of the acetone, adding the corresponding solvent.

The acetoxy analogues were incorporated by Sastre *et al.* [48, 49] in polymethyl methacrylate (PXAc/PMMA) as dopants and the analogues with a polymerizable group were copolymerized with methyl methacrylate (PXMA-MMA). PM567 was also incorporated in copolymers of MMA and different cross-linking

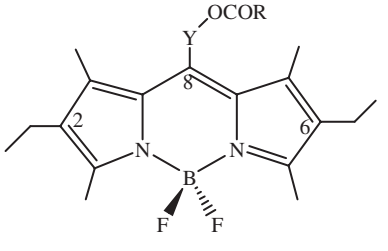


| Linear | R | Y = $(CH_2)X$ |
|---|---|---|
| PXAc | $CH_3$ | X = 1,3,5,10,15 |
| PXMA | $C(CH_3)=CH_2$ | X = 1,3,5,10,15 |

| Aromatic | R | Y=  $(CH_2)X$ |
|---|---|---|
| PArXAc | $CH_3$ | X = 1,3 |
| PArXMA | $C(CH_3)=CH_2$ | X = 1,3 |

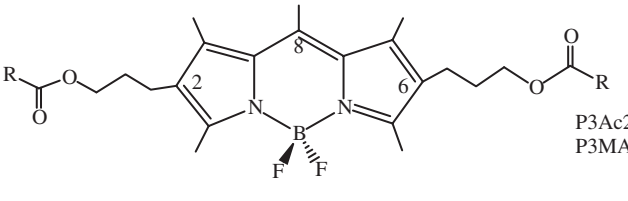


P3Ac2: R = $CH_3$
P3MA2: R = $C(CH_3)=CH_2$

Scheme 2. Molecular structures of polymerizable (PXMA and PArXMA) and acetoxy (PXAc and PArXAc) analogues [48, 49] of PM567 dye.

comonomers [47]. Disks of 10 mm diameter and 0.2 mm thickness for the analogues and 0.5 mm for PM567 were manufactured for solid-sample measurements [47–49]. The dye concentration was $1.5 \times 10^{-3}$ M and in some cases was decreased to $0.6 \times 10^{-3}$ (P15Ac and P15MA) and $0.45 \times 10^{-3}$ M (P1Ac and P1MA).

### 2.2. *Instrumental*

UV–Vis absorption and fluorescence (after excitation at the vibronic shoulder of the main absorption band) spectra were recorded on a Varian model CARY 4E spectrophotometer and a Shimadzu RF-5000 spectrofluorimeter, respectively. From the area under the absorption band, the oscillator strength ($f$) was obtained by means of:

$$f = \frac{4.39 \times 10^{-9}}{n} \int \varepsilon(\nu) \mathrm{d}\nu \tag{1}$$

where $\varepsilon(\nu)$ is the molar absorption coefficient at any wavenumber ($\nu$ in $\mathrm{cm}^{-1}$) and $n$ is the refractive index of the solvent. Fluorescence spectra were corrected from the wavelength dependence on the monochromator transmission and on the photomultiplier sensibility. The fluorescence quantum yield ($\phi$) was obtained using a diluted solution of rhodamine 110 in ethanol as reference ($\phi = 0.99$ at 20°C) [50]. The $\phi$ value was determined from the area under the emission band ($A_{\mathrm{fl}}$) and the intensity of the absorbed light at the excitation wavelength ($I_{\mathrm{ab}}(\lambda_{\mathrm{exc}})$) of both the sample and the reference (superscript r) by means of:

$$\phi = \phi^{\mathrm{r}} \frac{(n)^2}{(n^r)^2} \frac{I^{\mathrm{r}}_{\mathrm{ab}}(\lambda_{\mathrm{exc}})}{I_{\mathrm{ab}}(\lambda_{\mathrm{exc}})} \frac{A_{\mathrm{fl}}}{A^r_{\mathrm{fl}}} \tag{2}$$

where the effect of the refraction index ($n$) of the solvent was taken into account. In the polymeric samples, the reference was a solid disk of PM567 in a copolymer of trifluoromethyl methacrylate (30%) and MMA (70%) ($\phi = 0.64$) [51].

Radiative deactivation curves were recorded by means of the time-correlated single-photon counting technique with a time resolution of nanoseconds (Edinburgh Instruments model, $\eta$F900) and picoseconds (Edinburgh Instruments, model FL920). Emission was monitored at the fluorescence maximum after excitation by means of a hydrogen flash lamp with 1.5 ns FWHM pulses and 40 kHz repetition rate (in the $\eta$F900 model) or after excitation by diode lasers of 375 nm, 410 nm or 440 nm (PicoQuant models LDH375, LDH410 and LDH440) with around 150 ps FWHM and 10 MHz repetition rate (in the FL920 model). The measured fluorescence decay curves were deconvoluted from the pulse signal (registered by a Ludox suspension) by means of an iterative method of non-linear least squares based on the Marquardt algorithm. The decay curves were adjusted to a sum of exponentials by means of:

$$I_{\mathrm{fl}}(t) = A_1 \exp\left(\frac{-t}{\tau_1}\right) + A_2 \exp\left(\frac{-t}{\tau_2}\right) + \cdots \tag{3}$$

where $A_i$ are the pre-exponential factors related to the statistical weight of each exponential and $\tau_i$ are the lifetimes of each exponential decay. The goodness of the deconvolution process was controlled by the chi-squared ($\chi^2$) and Durbin–Watson (DW) statistical parameters and the distribution of the residuals.

For high optical density samples (concentrated solutions and polymeric samples) the front-face (reflection) configuration was used to record the fluorescence signal, orientating the sample to 35° and 55° with respect to the excitation beam and emission arm, respectively. In concentrated solutions (up to $2 \times 10^{-3}$ M) cuvettes of short optical pathways (0.1, 0.01 and 0.001 cm) were employed.

The rate constants of radiative ($k_{fl}$) and non-radiative ($k_{nr}$) deactivation pathways were calculated by means of: $k_{fl} = \phi/\tau$ and $k_{nr} = (1-\phi)/\tau$. All measurements were carried out in aerated samples. The temperature of the samples was controlled by an external flow of thermostatized water.

### 2.3. *Computational*



Quantum mechanical calculations were performed at the semiempirical, *ab initio* and density functional theory (DFT) [52] levels. The ground state geometry obtained at the DFT level (implemented in the Gaussian 03 software) [53] was calculated with the B3LYP [54, 55] method and the 6-31G basis set (adding polarization and diffuse functions in some cases) and the default options for convergence. In the semiempirical calculations, the AM1 [56] and PM5 methods (incorporated in the MOPAC 2002 software) [57] were employed, imposing the minimum gradient for convergence at 0.01 kcal mol$^{-1}$ Å$^{-1}$ and using the eigenvector-following routine. The first excited singlet state geometry was obtained with the *ab initio* Configuration Interaction Singles (CIS) [58] and semiempirical Configuration Interaction Singles and Doubles (CISD/AM1) methods (considering eight molecular orbitals in the active space). In all cases, no geometrical restrictions were imposed during the optimization procedure and a geometry was considered as optimized when the analysis of the vibrational frequencies did not give any negative value.

The absorption characteristics (energy gap $\Delta E_{ab}$ and oscillator strength $f$) were calculated by means of the transition from the optimized ground state to the Franck–Condon excited states ($S_0 \rightarrow S_1, S_2, \ldots$), while the fluorescence properties (energy gap $\Delta E_{fl}$ and radiative deactivation rate $k_{fl}$) were calculated for the transition from the first optimized excited state to the Franck–Condon ground state ($S_1 \rightarrow S_0$). The $k_{fl}$ value was obtained from the corresponding $S_1 \rightarrow S_0$ oscillator strength by means of:

$$k_{fl} = A_{S_1 \rightarrow S_0} = \frac{2\pi\nu^2 e^2}{c^3 m_e \varepsilon_0} f \tag{4}$$

where $A$ is the Einstein spontaneous emission coefficient; $\nu$ is the calculated emission wavenumber; $e$ and $m_e$ are the electron charge and mass, respectively; $c$ is the light speed and $\varepsilon_0$ is the vacuum dielectric constant. The spectral characteristics are determined by the time dependent (TD-DFT) [59] and the semiempirical

Zerner's Intermediate Neglect of Differential Overlap (ZINDO) [60] and CISD/AM1 methods.

The solvent effect was also considered in the geometry optimization, charge distribution and spectral characteristics by means of the semiempirical Conductor-like Screening Model (COSMO) [61] together with the PM5 level, and the Self-Consistent Reaction Field (SCRF) together with the B3LYP method. The considered solvents are *c*-hexane (dielectric constant $\varepsilon = 2.0$) as apolar, acetone ($\varepsilon = 20.7$) as polar and methanol ($\varepsilon = 32.7$) as polar/protic. In the SCRF model, the solvent was simulated by the Polarizable Continuum Model (PCM) [62] theory. The optimization with the COSMO model was carried out considering a cavity radius of 5.65 Å, obtained from volume calculations at the B3LYP/6-31G level for PM567 dye, and a solvent radius of 3.50 Å for *c*-hexane, 3.07 Å for acetone and 2.52 Å for methanol [57].

## 3. Results and discussion

### 3.1. *Preliminary considerations. Molecular structure*



The basic structure of PM dyes consists of two pyrrole units linked by a methylene and a $BF_2$ group, providing rigidity to the chromophore system (scheme 1). Indeed, quantum mechanical calculations recognize the $C_{2v}$ point symmetry group for the optimized geometry of the PM chromophore, without any substituents, in the ground state. These results indicate a planar structure for the chromophore, which would provide strong absorption and fluorescence bands for PM dyes. The validity of the theoretical calculations is confirmed by X-ray diffraction data [63], since the geometrical parameters (bond lengths, angles and dihedral angles), experimentally obtained from the simplest commercially available PM dye (PM546, $R_2 = CH_3$, scheme 1), are very similar to those theoretically proposed by the DFT B3LYP method, with deviations not longer than 1.5% in bond lengths and 2° in bond angles [64]. Semiempirical calculations, although not so accurate, also adequately describe the geometry of the ground state.

PM dyes are neutral molecules, but with a zwitterionic structure in which a positive charge is delocalized through the electronic $\pi$-system. Quantum mechanical calculations localize the negative electronic density of the PM chromophore mainly in the F atoms and, to a lower extent, in the N atoms (figure 1). The B atom is tetracoordinated, so a net negative charge centred in this atom should be expected. However, theoretical results suggest a net positive charge in the B atom, which can be assigned to the high electronegativity of the F and N atoms directly linked to the B atom. As a result of the electronic charge delocalization through the conjugated $\pi$-system, PM dyes can be defined as cyclic polymethine- or cyanine-like structures [7, 12]. In fact, an alternative (positive and negative) charge distribution and the equalization of the C–C bond length through the delocalized $\pi$-system are observed. This last factor can be evaluated by the bond length alternation (BLA) [65] parameter defined as:

$$\mathrm{BLA} = \bar{L}_{C-C} - \bar{L}_{C=C} \tag{5}$$

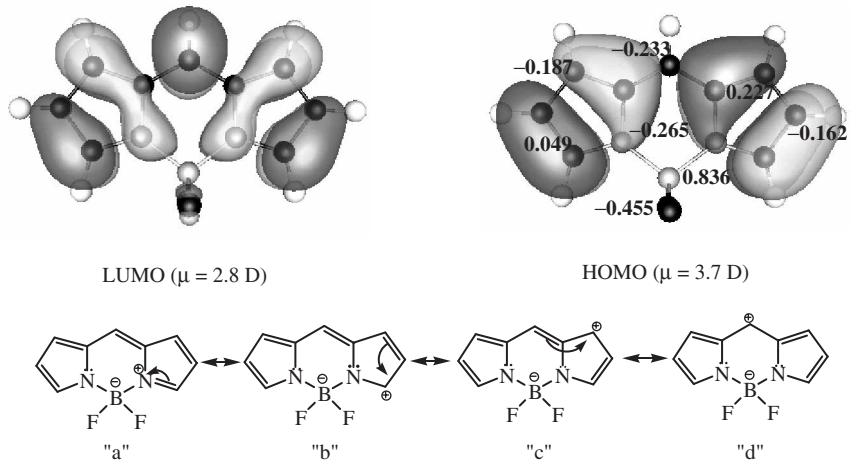


Figure 1. Contour maps of the electronic density of the HOMO and LUMO orbitals calculated by the B3LYP/6-31G method, including the Chelpg point charges and the dipole moment of PM546. The resonance structures are also enclosed.



where $L_{C-C}$ and $L_{C=C}$ are, respectively, the average bond length of alternative single and double bonds in the conjugated $\pi$-system. The chromophore can be described by the resonance structures (and their symmetrical counterparts) included in figure 1. Two extreme resonance structures can be considered: the structures '*a*', where the positive charge is localized at the N atoms; and the structure '*d*', where the localization of the positive charge at the central C atom provides a higher charge separation along the short molecular axis.

From the electronic distribution proposed by quantum mechanical calculations, the molecular dipole moment can be evaluated. The dipole moment of PM dyes is oriented along the short molecular axis because of $C_{2v}$ symmetry reasons. The relatively small dipole moment of PM dyes with respect to other dyes (theoretically predicted to be around 3D) should be attributed to the alternative charge distribution through the short molecular axis; for instance, the positive charge localized at the B atom is enclosed between electronegative atoms (F and N atoms). On the other hand, theoretical calculations suggest that the dipole moment in the HOMO state is higher than in the LUMO state; for instance, the dipole moment of the PM546 dye decreases from $\mu(\text{HOMO}) = 3.7\,\text{D}$ to $\mu(\text{LUMO}) = 2.8\,\text{D}$ upon excitation (figure 1) [66]. Therefore, the resonance structure '*a*', with a low charge separation along the short molecular axis, has a lower statistical weight in the HOMO state than in the LUMO state, while the canonical form '*d*' is more dominant in the LUMO and in the HOMO state (figure 1).

The $BF_2$ group acts as a linking bridge. It does not take part in the delocalized $\pi$-system but provides rigidity to the molecular structure, reducing the electron flow in the aromatic ring, i.e. disrupting the electronic loop [1]. Consequently PM dyes can be classified as quasi-aromatic dyes [15], characterized by a low intersystem crossing probability by means of the 'Drexhage's loop rule' [1]. This effect implies a significant advantage of PM dyes with respect to other laser dyes, since the reduction in the

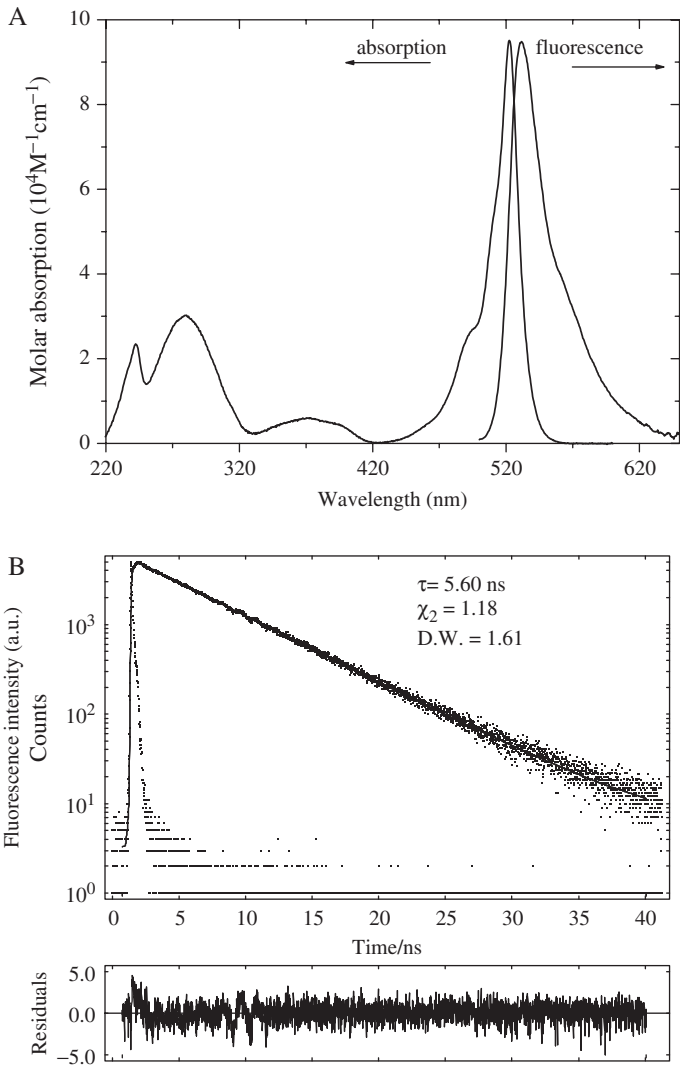


Figure 2. Absorption and fluorescence spectra (A) and fluorescence decay curve (B, analysed as one exponential) of PM567 ($2 \times 10^{-6}$ M) in c-hexane.

population of the long-life $T_1$ triplet state by the intersystem crossing process would decrease the triplet–triplet absorption, one of the most important losses in the resonator cavity. Therefore, it is expected that PM dyes yield high lasing efficiencies.

### 3.2. *General photophysics*

Figure 2(A) shows an illustrative example of the UV–Vis absorption and fluorescence spectra of a diluted solution of PM567 in *c*-hexane. Except in the cases of substituents with important electron donor/acceptor capacities or aromatic groups which can

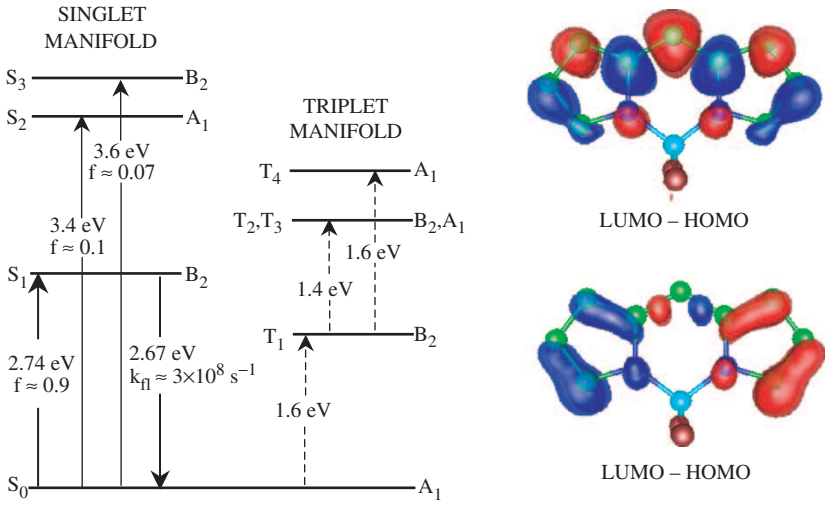


Figure 3. Electronic excited states of PM chromophore characterized by the $C_{2v}$ symmetry point group: energy gap ($\Delta E$ in eV), oscillator strength ($f$) and radiative rate constant ($k_{fl}$, in $s^{-1}$) calculated by the ZINDO method. The difference and product of the electronic density of the LUMO and HOMO orbitals, showing the change of the dipole moment upon excitation and the transition density, are also included.



produce important changes in the photophysics of PM dyes, the absorption and fluorescence characteristics of PM dyes do not extensively depend on the nature of the substituents and/or the solvent. [19, 36] The lowest energy absorption band, the transition from the ground to the first excited state ($S_0 \rightarrow S_1$), is centred at around 520 nm, in the green part of the visible region, with a molar absorption coefficient $\varepsilon \approx 9 \times 10^4\,M^{-1}\,cm^{-1}$ (or oscillator strength $f \approx 0.5$). It presents a shoulder at higher energies (at around 1100 $cm^{-1}$ from the maximum), which can be assigned to out-of-plane vibrations of the aromatic C–H skeleton. Other absorption bands, transitions to higher singlet excited states ($S_2$, $S_3$, ...), are much less intense than the $S_0 \rightarrow S_1$ transition (figure 2A).

The energy diagram, provided by quantum mechanical calculations on the basis of the $C_{2v}$ symmetry point group (figure 3), suggests that the $S_0 \rightarrow S_1$ band corresponds to an allowed $A_1 \rightarrow B_2$ transition, which is polarized along the long molecular axis. The absorption bands to higher excited states would correspond to less probable $A_1 \rightarrow A_1$ and $A_1 \rightarrow B_2$ transitions. Quantum mechanical calculations also suggest that the $S_0 \rightarrow S_1$ transition is nearly a promotion of an electron from the HOMO orbital to the LUMO orbital obtained from the optimized geometry in the $S_0$ state, where the electronic density is localized mainly at the central C atom (figure 1). The difference of the electronic density of both orbitals (LUMO-HOMO in figure 3) indicates that the excitation implies a change in the dipole moment along the short molecular axis, which is consistent with the diminution in the dipole moment upon excitation, discussed above. On the other hand, the transition density, obtained by the multiplication of the electronic density of both orbitals (HOMO · LUMO in figure 3), corroborates that the $S_0 \rightarrow S_1$ transition is polarized along the long molecular axis [64, 66, 67].

The fluorescence spectrum is practically the mirror image of the $S_0 \rightarrow S_1$ absorption band (figure 2A), suggesting the similarity between the vibrational levels of the $S_0$ and $S_1$ states. The emission band is placed at around 535 nm, with a low Stokes shift ($\approx 500\,cm^{-1}$). Theoretical calculations suggest that the optimized geometry for the $S_1$ excited state is quite similar to that obtained for the $S_0$ ground state, validating the experimentally observed small Stokes shift. The shape of the fluorescence band is independent of the excitation wavelength indicating that the emission is from the lowest vibrational level of the $S_1$ excited state. This emission band is characterized by an important fluorescence quantum yield ($\phi \approx 0.7$) and, depending on the nature of the substituent and the solvent, PM dyes can fluoresce with a quantum yield close to the unit. The $\phi$ value is independent of the excitation wavelength, suggesting that, in spite of the populated excited state ($S_2, S_3, \ldots$), they rapidly deactivate to the fluorescent lowest excited state.

In most cases, the fluorescence decay curves of PM dyes can be analysed as one exponential decay with a lifetime around 5–6 ns, as is illustrated in figure 2(B) for the specific case of a diluted solution of PM567 in *c*-hexane. The fluorescence lifetime of PM dyes is observed to be independent of the excited and emission wavelengths. In viscous solvents the decay curves are analysed with a second component, a growing contribution (negative pre-exponential) with a short lifetime ($< 0.50$ ns). However, when these curves are registered at the magic angle conditions (emission polarizer at 54.7° with respect to the plane polarized excitation), the second contribution disappears, indicating that the growing component is due to the rearrangement of the solvent molecules during the lifetime of the $S_1$ state, i.e. to accommodate the solvation shells to the change in the dipole moment of the dye molecules after excitation.

Table 1 lists the photophysical characteristics of diluted solutions of PM546, together with the theoretically calculated values in the gas phase by two representative quantum mechanical calculations: a semiempirical ZINDO and an *ab initio* TD-DFT method. The semiempirical methods predict the best values for the energy gap with respect to those experimentally observed, probably because the semiempirical methods are parameterized to reproduce the experimental values. Although the *ab initio* methods overestimate the energy gap, they satisfactorily reproduce the absorption

Table 1. Photophysical properties of PM546 in diluted solutions ($2 \times 10^{-6}$ M) of c-hexane, acetone and methanol: absorption and fluorescence wavelengths ($\lambda_{ab}$ and $\lambda_{fl}$), molar absorption coefficient ($\varepsilon$), oscillator strength ($f$), Stokes shift ($\Delta\nu_{St}$), fluorescence quantum yield ($\phi$) and lifetime ($\tau$), and radiative ($k_{fl}$) and non-radiative ($k_{nr}$) deactivation rate constants. The theoretical results calculated by the semiempirical ZINDO and the *ab initio* TD-B3LYP methods are also included.

| | *c*-hexane [68] | Acetone [68] | Methanol [68] | ZINDO [64] | TD-B3LYP [64] |
|---|---|---|---|---|---|
| $\lambda_{ab}$ (±0.1 nm) | 499 | 493 | 492 | 479 | 403 |
| $\varepsilon$ ($10^4\,M^{-1}\,cm^{-1}$) | 9.74 | 7.86 | 8.21 | – | – |
| $f$ | 0.45 | 0.40 | 0.46 | 0.86 | 0.53 |
| $\lambda_{fl}$ (±0.4 nm) | 509 | 504 | 504 | 484 | 407 |
| $\Delta\nu_{St}$ ($cm^{-1}$) | 400 | 425 | 455 | 235 | 215 |
| $\phi$ (±0.05) | 0.77 | 0.93 | 0.95 | – | – |
| $\tau$ (±0.05 ns) | 5.23 | 5.55 | 5.58 | – | – |
| $k_{fl}$ ($10^8\,s^{-1}$) | 1.47 | 1.68 | 1.61 | 2.41 | 1.88 |
| $k_{nr}$ ($10^8\,s^{-1}$) | 0.45 | 0.30 | 0.20 | – | – |

and fluorescence transition moments, evaluated by the oscillator strength ($f$) and the radiative rate constant ($k_{fl}$), respectively. Besides, the light spectral shifts and changes in the transition moments by the effect of the substituents and the solvent are more accurately predicted by *ab initio* than by semiempirical methods. These results emphasize the complementary nature of semiempirical and *ab initio* methods to best predict the absorption and fluorescence properties of PM dyes. The photophysical characteristics of PM dyes are similar to those of rhodamine dyes, probably the most-used active media for tunable dye lasers [19].

On the other hand, taking into account that the active media of dye lasers need high optical density samples to record the laser signal, it is of great interest to register the photophysical properties of PM dyes in highly concentrated solutions. The shape of the absorption band of PM dyes is nearly independent of the dye concentration (at least up to $2 \times 10^{-3}$ M), as shown in figure 4. The non-observation of any methachromasy effect at high dye concentrations suggests the absence of dye aggregation of PMs in this concentration range. The low tendency to self-associate presents a great photophysical advantage of these dyes with respect to rhodamine dyes as active media of tunable lasers [19]. Indeed, rhodamine dyes have a high tendency to self-aggregate (the methachromasy effect in the absorption spectra) and aggregates are formed at moderate concentrations in liquid solutions. These non-fluorescent aggregates are efficient quenchers of the fluorescent emission of the monomers, drastically reducing the fluorescence capacity of rhodamines in concentrated solutions [16, 19].



The fluorescent band and decay curves of PM dyes, however, present an important dependence on the dye concentration (figure 4), even if a front-face configuration with a 1 mm optical path cuvette is used to record the fluorescent emission. Indeed, an increase in the dye concentration leads to a bathochromic shift in the fluorescent band, a decrease of its intensity and an augmentation of its lifetime. These changes depend on the optical pathway of the used cuvette and the fluorescence properties with a 0.01 mm pathway cell tend to return to the observed spectra and values obtained in diluted solutions with 1 cm cuvettes in the right-angle configuration. These observations indicate that the dependence of the fluorescence signals on the dye concentration is due to the inner filter (i.e. reabsorption/remission effects), and confirms the low tendency of PM dyes to self-aggregate. Present results suggest the convenience of using diluted dye solutions to register the intrinsic photophysical properties of dyes in solution. The reabsorption/reemission effects observed in the experimental spectra recorded in the 0.1 and 1 mm cuvettes can be corrected by mathematical procedures [18].

### 3.3. *2,6-Disubstituted-pyrromethenes*

In this section the photophysics of pyrromethenes with a methyl group at the 8 position (PM546) and different substituents at the 2 and 6 positions, such as sulfonate (PM556), ethyl (PM567) and *tert*-butyl (PM597) groups, are analysed (scheme 1). The study is carried out in a multitude of apolar, polar and protic solvents.

As shown in figure 5, both the absorption and fluorescence bands of PMs shift to lower energies and decrease the intensity due to the presence of the alkyl and

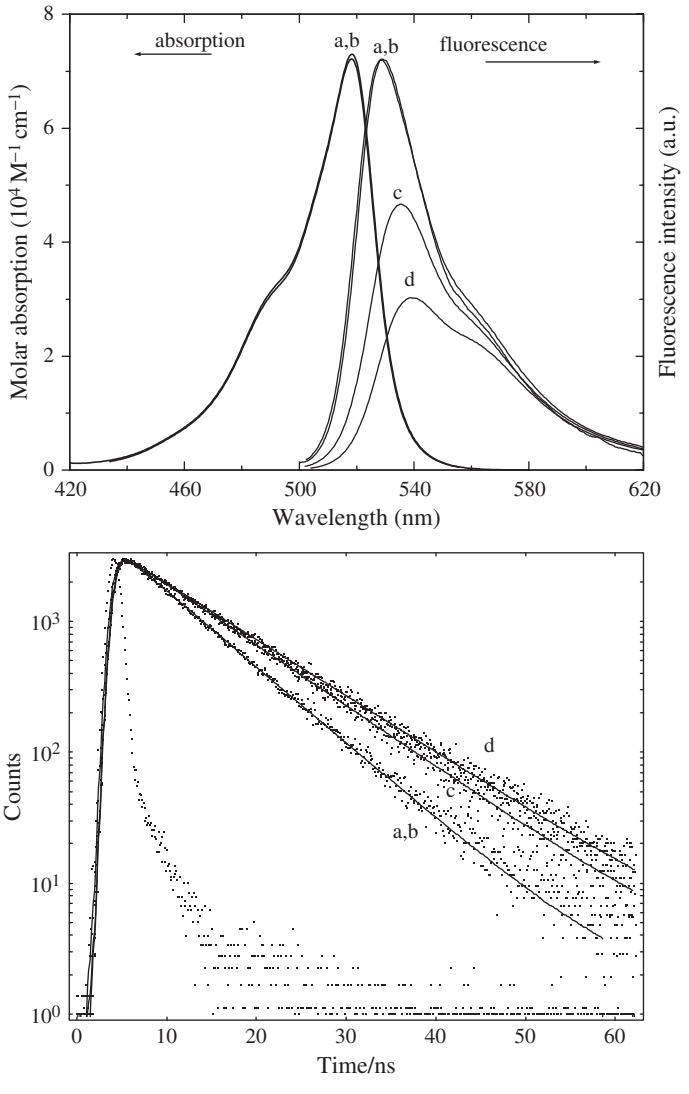


Figure 4. Absorption and fluorescence spectra and fluorescence decay curves of PM567 in diluted (a, $2 \times 10^{-6}$ M and l = 1 cm) and concentrated (b, $2 \times 10^{-3}$ M and l = 0.001 cm) solutions of $F_3$-ethanol. The fluorescence spectra and decay curves at $2 \times 10^{-3}$ M but with cuvettes of 0.01 cm (c) and 0.1 cm (d) pathways are also included.

sulfonate groups. The fluorescence lifetime shows a non-clear evolution. The corresponding photophysical characteristics of alkyl and sulfonate PM dyes in a common solvent are summarized in table 2. The theoretical methods adequately reproduce the bathochromic shift in the spectral bands and the diminution in the transition probabilities due to the presence of alkyl or sulfonate groups at the 2 and 6 positions of the PM chromophore. TD-DFT stands out as the best calculation method to describe the effect of the substituent on the photophysics of PM dyes (table 2). The substituents

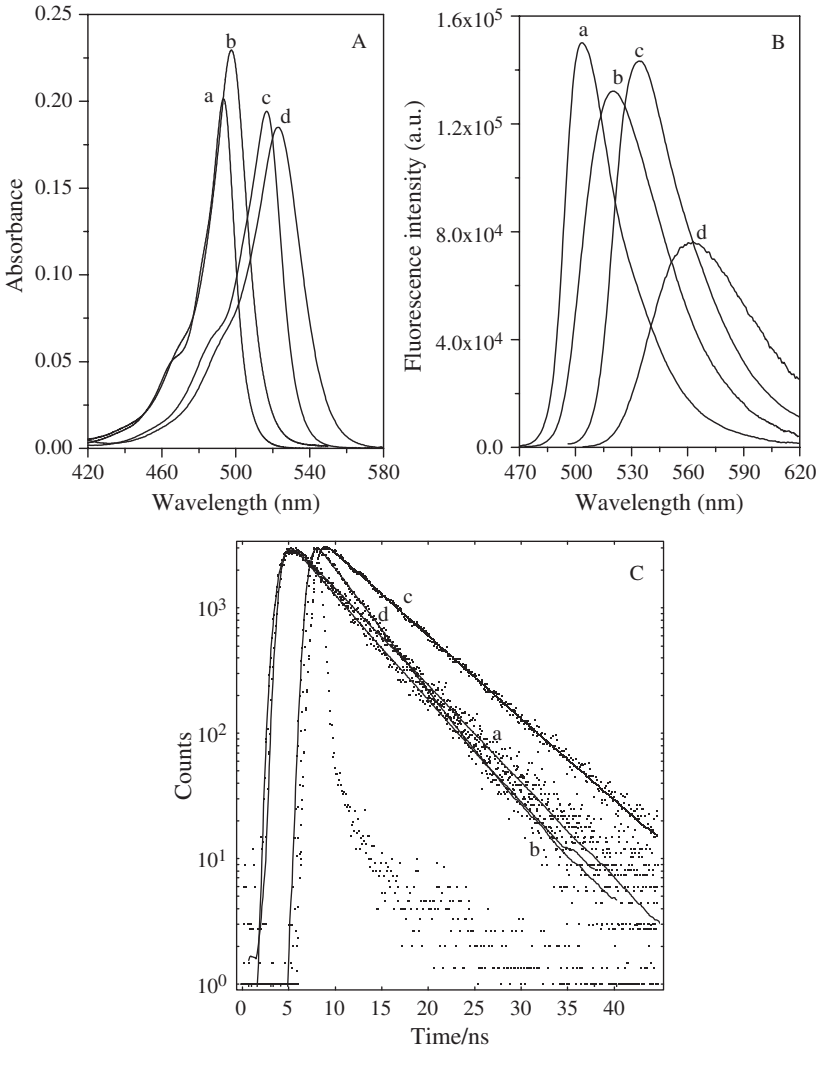


Figure 5. Absorption (A) and fluorescence (B) spectra, and fluorescence decay curves (C) of PM546 (a), PM556 (b), PM567 (c) and PM597 (d) in diluted solutions ($2 \times 10^{-6}$ M) of methanol.

can affect the spectral band positions by several phenomena, such as the inductive effect, the resonant interaction and the hyperconjugation. The resonant effect is not present in alkyl substituents, and the fact that the spectral shifts are higher by the *t*-butyl units (around 30 nm) than by the ethyl groups (around 25 nm), suggests a more important influence of the inductive than the hyperconjugation effect. In spite of the electronegativity of S and O atoms, the resonant interaction predominates in the sulfonate groups. Consequently, both the resonant and the inductive effects shift the spectral bands to lower energies, which can be explained by the higher electronic density at the 2 and 6 positions in the HOMO than in the LUMO orbitals, as is

Table 2. Experimental (in methanol) and theoretically predicted photophysics of PM546, PM556, PM567 and PM597 dyes in diluted solutions ($2 \times 10^{-6}$ M). The lasing efficiency (%Eff) in high concentrated solutions ($\approx 10^{-3}$ M) is also included.

| | | PM546 [68] | PM556 [69] | PM567 [45] | PM597 [70] |
|---|---|---|---|---|---|
| Experimental (methanol) | $\lambda_{ab}$ (nm) | 492 | 498 | 516 | 523 |
| | $\varepsilon$ ($10^4$ $M^{-1}$ $cm^{-1}$) | 8.21 | 9.44 | 7.90 | 7.58 |
| | $f$ | 0.46 | 0.43 | 0.49 | 0.38 |
| | $\lambda_{fl}$ (nm) | 504 | 525 | 532 | 561 |
| | $\Delta\nu_{St}$ ($cm^{-1}$) | 455 | 1055 | 560 | 1305 |
| | $\phi$ | 0.95 | 0.84 | 0.91 | 0.48 |
| | %Eff* | – | – | 51.0 | 47.6 |
| | $\tau$ (ns) | 5.58 | 4.78 | 6.10 | 4.21 |
| | $k_{fl}$ ($10^8$ $s^{-1}$) | 1.71 | 1.76 | 1.49 | 1.14 |
| | $k_{nr}$ ($10^8$ $s^{-1}$) | 0.09 | 0.34 | 0.14 | 1.23 |
| ZINDO | $\lambda_{ab}$ (nm) | 479 | – | 492 | 494 |
| | $f$ | 0.86 | – | 0.88 | 0.87 |
| | $\lambda_{fl}$ (nm) | 484 | – | 500 | 516 |
| | $\Delta\nu_{St}$ ($cm^{-1}$) | 235 | – | 335 | 915 |
| | $k_{fl}$ ($10^8$ $s^{-1}$) | 2.41 | – | 2.21 | 2.08 |
| TD-B3LYP | $\lambda_{ab}$ (nm) | 403 | – | 426 | 429 |
| | $f$ | 0.53 | – | 0.54 | 0.52 |
| | $\lambda_{fl}$ (nm) | 407 | – | 433 | 455 |
| | $\Delta\nu_{St}$ ($cm^{-1}$) | 215 | – | 360 | 1365 |
| | $k_{fl}$ ($10^8$ $s^{-1}$) | 1.88 | – | 1.60 | 1.61 |

*[PM567] $= 9 \times 10^{-4}$ M and [PM597] $= 8 \times 10^{-4}$ in ethanol [71].



predicted by quantum mechanical calculations (figure 1). Therefore, an electron donor substituent at these positions more extensively destabilizes the HOMO than the LUMO states, leading to a reduction in the $S_0$–$S_1$ energy gap.

On the other hand, all PM dyes show similar probabilities for the $S_0$–$S_1$ transitions ($f$ and $k_{fl}$ values), but the PM597 dye presents a higher non-radiative rate constant, $k_{nr}$ value, with respect to the other PM dyes (table 2). Owing to the low probability of intersystem crossing of PM dyes [15, 38, 39], the non-radiative deactivation processes are assigned to the internal conversion mechanisms, which are related, among with other factors, to the flexibility/rigidity of the aromatic $\pi$-system of the chromophore [1]. Some authors have related the flexibility of PM chromophores with the planarity of their electronic $\pi$-system [28, 37]. Therefore, a loss of planarity in the $S_1$ state, for instance by the presence of bulky *t*-butyl groups, could imply an increase in the internal conversion processes of PM dyes, explaining the observed reduction in the fluorescence capacity of PM597. This fact is confirmed by quantum mechanical calculations, since they predict a loss of planarity in the pyrrole units of the PM597 in the excited state with respect to the PM567 dye (i.e. the dihedral angle between the C atoms at the 5, 6, 7 positions and the adjacent C atom, $\alpha(C_5–C_6–C_7–C)$, is 4.7° for PM597 versus 0.2° for PM567) [70]. This disruption from planarity should be attributed to the steric hindrance between the bulky *t*-butyl groups (2 and 6 positions) with the adjacent methyl groups (1 and 3, and 5 and 7, respectively), since quantum mechanical calculations do not predict any loss in planarity by the presence of the *t*-butyl group at the 2 and 6 positions for the PM chromophore without any methyl substituent at the

1, 3, 5 and 7 positions. The disruption in the planarity of the PM597 derivative would imply an extra bathochromic shift in the fluorescence band (with respect to the absorption band) and, consequently, an increase of the Stokes shift (table 2).

**3.3.1. Solvent effect.** The presence of alkyl or sulfonate groups in PM dyes makes this chromophore compatible with all organic and aqueous solvents. Thus, the PM556 derivative is soluble in water, water/ethanol mixtures and most of the alcohols [69], whereas PM546, PM567 and PM597 dyes are soluble in all apolar, polar and protic solvents, and in some alcohol-rich water/ethanol mixtures [21, 45, 70]. The photophysical properties of commercial PM dyes have been studied in a wide variety of apolar, polar and protic solvents and mixtures of water/ethanol. In all derivatives, the same tendencies are experimentally observed and theoretically predicted for the effect of the solvent on the absorption and fluorescent characteristic of PM dyes; in general, the spectral bands shift to higher energies and the fluorescence capacity and lifetime increase in polar media, mainly due to a diminution in the non-radiative deactivation. Again, the TD-DFT method in combination with the PCM solvation model is the most accurate quantum mechanical calculation describing the solvent effect on the photophysics of PMs [73].



The evolution of the photophysical properties can be analysed by the Lippert $\Delta f$ parameter, which accounts for the polarity/polarizability of the solvent by means of the dielectric constant ($\varepsilon$) and the refractive index ($n$) of the solvent [$\Delta f = (\varepsilon - 1)/(2\varepsilon + 1) - (n^2 - 1)/(2n^2 + 1)$], or the Reichardt $E_T^N(30)$ parameter, which describes the polarity/polarizability and acidity of the solvent by means of the observed shift in the absorption band of a betaine dye used as a molecular probe. However, the most precise description of the solvent effect is a multilinear correlation analysis, where a physicochemical property ($XYZ$) is simultaneously correlated with different solvent properties ($A$, $B$, $C$, ...) by means of [76–81]:

$$(XYZ) = (XYZ)_0 + c_a A + c_b B + c_c C + \cdots \tag{6}$$

where $(XYZ)_0$ is the physicochemical property of interest in an inert solvent and $c_a$, $c_b$, $c_c$, ... are the adjusted coefficients, which reflect the dependence of the corresponding $A$, $B$, $C$, ... solvent parameters. The most general solvent parameters affecting the absorption and fluorescence properties of conjugated $\pi$-systems are the polarity/polarizability, the H-bond donor/acceptor capacity and the electron-releasing ability. These factors are described by Taft ($\pi^*$-, $\alpha$- and $\beta$-scales, respectively) [76–78] and Catalan ($SPP^N$-, SA- and SB-scales, respectively) parameters [79–81]. The multilinear analysis obtained for the main photophysical properties of PM597 dye are shown in figure 6, and the corresponding adjusted coefficients are summarized in table 3. Both absorption and fluorescence bands shift to higher energies by increasing the solvent polarity/polarizability ($c_{\pi^*} > 0$ for $\nu_{ab}$ and $\nu_{fl}$ in table 3), while the solvent basicity induces light spectral shifts toward lower energies ($c_\beta \leq 0$). The effect of the solvent acidity on the position of the spectral bands is practically negligible ($c_\alpha \approx 0$). These results experimentally confirm the decrease in the dipole moment of PM dyes upon excitation, as is theoretically predicted by quantum mechanical calculations.

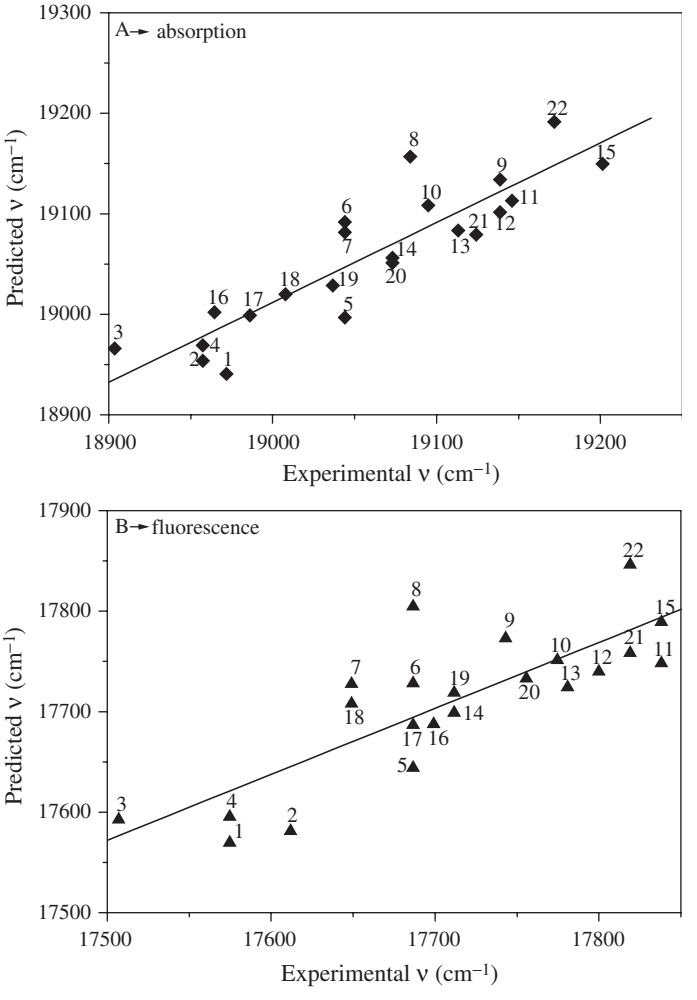


Figure 6. Correlation between the experimental absorption (A) and fluorescence (B) wavenumber and the values predicted by means of a multilineal regression analysis (equation 6) using the Taft $\pi^*$-, $\alpha$- and $\beta$-solvent parameters [76–78]. Apolar (1–4), polar/aprotic (5–15) and polar/protic (16–22) solvents [70].

On the other hand, the $k_{fl}$ value of alkyl-PMs is nearly solvent-independent, while the $k_{nr}$ value decreases in polar solvents (table 3). A possible explanation for the reduction in the internal conversion of alkyl-PM dyes in polar/protic media, previously applied to rhodamines and 7-amino-coumarines, should be related to the electron flow and the delocalization of the positive charge through the $\pi$-system of the PM chromophore, represented as the interconversion between the two extreme resonance structures '*a*' and '*d*' of figure 1 [72]. Thus, an electrostatic stabilization of the positive charge with the dielectric constant of the solvent or any specific solute–solvent interaction reducing the charge mobility through the conjugated $\pi$-system, should lead to a diminution in the non-radiative deactivation and an increase in the fluorescence capacity of alkyl-PMs in polar/protic solvents.

Table 3. Adjusted coefficients ($(XYZ)_0$, $c_{\pi^*}$, $c_\alpha$ and $c_\beta$) of the multilinear regression analysis (equation 6) for the absorption ($\nu_{ab}$) and fluorescence ($\nu_{fl}$) wavenumber, and the radiative ($k_{fl}$) and non-radiative deactivation ($k_{nr}$) constant of PM597 [70] with the solvent polarity/polarizability, acidity and basicity described by the Taft ($\pi^*$, $\alpha$ and $\beta$) scales [76–78].

| *XYZ* | $(XYZ)_0$ | $c_{\pi^*}$ | $c_\alpha$ | $c_\beta$ |
|---|---|---|---|---|
| $\nu_{ab}$ ($cm^{-1}$) | 18970 (±20) | 300 (± 40) | – | −110 (± 35) |
| $\nu_{fl}$ ($cm^{-1}$) | 17590 (±25) | 280 (± 50) | 30 (± 25) | −50 (±50) |
| $\ln(k_{fl})$ | 18.35 (±0.05) | 0.16 (±0.11) | – | −0.18 (±0.10) |
| $\ln(k_{nr})$ | 18.75 (±0.04) | −0.20 (±0.08) | −0.05 (±0.04) | 0.11 (±0.08) |

**3.3.2. Photophysics-lasing correlations.** The photophysical properties of alkyl-PM dyes satisfactorily correlate with their laser performance by changing both the substituent and the solvent (table 2). The presence of *t*-butyl groups instead of ethyl groups (PM597 vs. PM567) reduces the lasing efficiency [71], which correlates with a diminution in the fluorescence quantum yield of PM dyes. However, the decrease in the lasing efficiency is not so pronounced, probably due to the higher Stokes shift in PM597 vs. PM567 which reduces the losses of the resonator cavity [70]. On the other hand, figure 7 shows the satisfactory correlation between the photophysical and lasing properties [45] for PM567 in a multitude of solvents; indeed, the fluorescence and lasing bands shift to higher energies by increasing the solvent polarity (the corresponding wavenumbers show a linear correlation), whereas the increase in the lasing efficiency in polar protic solvents inversely correlates with the reduction in the non-radiative deactivation rate constant. Similar results are obtained for other PM derivatives in some representative apolar, polar and protic solvents [46]. Therefore, experimental results recommend polar/protic media as the best environmental conditions to get the most efficient fluorescent and laser performances for alkyl-PM dyes.

Present results suggest the viability of the photophysical properties to predict the best structural and environmental conditions to optimize the laser performance of alkyl-PM dyes. Moreover, taking into account the accuracy of the quantum mechanical calculations to predict the effect of the substituents and the solvent on the photophysics of these dyes, it can be considered as a helpful tool of the theoretical calculations to orientate the modelization of the new molecular structures of PM dyes with specific photophysical properties, and consequently with predesigned lasing characteristics.

**3.3.3. PM567 in polymeric matrices: cross-linking effect.** PM567 dye was incorporated [47] in a solid polymethyl methacrylate (PMMA) matrix (scheme 3), which is characterized by its good transparency to visible radiation. Table 4 summarizes the photophysical properties of PM567 in PMMA and in ethyl acetate, a liquid solvent with similar physicochemical properties to those of the solid host material. The position of the absorption band of PM567 in PMMA is similar to that obtained in polar media, confirming that the polymeric matrix provides a polar environment due to the presence of the pendant methoxycarbonyl groups. This is an important characteristic since the highest fluorescence quantum yields and lasing efficiencies of PM567 are achieved

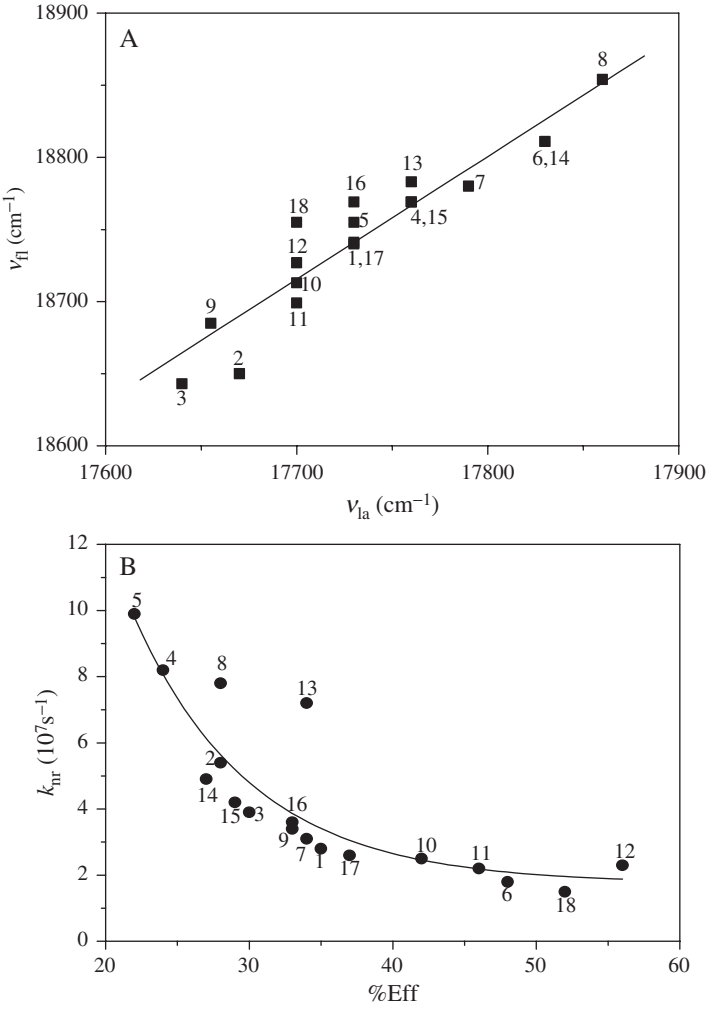


Figure 7. Correlation between: (A) fluorescence ($\nu_{fl}$) and lasing ($\nu_{la}$) [45] wavenumber, and (B) the non-radiative deactivation rate constant ($k_{nr}$) and lasing efficiency (%Eff) [45] of PM567 in several apolar (1–4), polar (5–11) and polar/protic (12–18) solvents [45].

in polar media. The shape of the absorption spectrum in the solid phase is wider than in the liquid media. However this fact is independent of the dye concentration in the polymeric matrix, therefore it is not due to methachromasy effects, which enhances the losses in the resonator cavity. Probably, this widening is due to the modification of the vibrational structure of the spectra as a result of the higher rigidity of the solid matrix. Although the registered fluorescence properties of these dyes in the solid matrix are affected by the reabsorption and reemission effects (optical density at the excitation wavelength around 0.8 for solid disk thickness around 0.2 mm), the correction of the effect by mathematical procedures [18] leads to corrected fluorescence

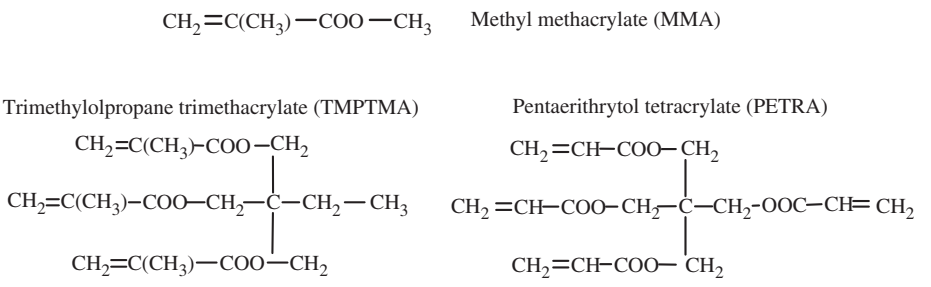


Scheme 3. Polymerizable acrylic and methacrylic monomers [47].

Table 4. Photophysics of PM567 in PMMA ($1.5 \times 10^{-3}$ M and thickness of 0.2 mm) and in ethyl acetate ($2 \times 10^{-3}$ M and cuvettes of 0.01 mm). The fluorescence parameters of the polymeric samples are corrected from the reabsorption and reemission phenomena (c superscript) [18].

| | $\lambda_{ab}$ (nm) | $\lambda_{fl}^{c}$ (nm) | $f$ | $\phi^{c}$ | $\tau^{c}$ (ns) | $k_{fl}$ ($10^{8}$ s$^{-1}$) | $k_{nr}$ ($10^{8}$s$^{-1}$) |
|---|---|---|---|---|---|---|---|
| PMMA [82] | 518.5 | 531.0 | 0.47 | 0.63 | 7.52 | 0.83 | 0.49 |
| Ethyl acetate [45] | 516.7 | 534.0 | 0.55 | 0.83 | 5.99 | 1.38 | 0.28 |



parameters similar to those obtained in diluted PM567 solution of polar media. Therefore, solid polymer matrices do not drastically change the photophysical properties of PM dyes, although it has been observed that solid materials offer an important improvement in the thermal and photostability of the dye [49, 82].

The rigidity of the polymer PMMA matrix can be modified by adding adequate cross-linking agents [47]. The reduction in the free volume surrounding the PMMA matrix by the copolymerization of MMA and different cross-linking agents, illustrated in scheme 3, enhances the fluorescence capacity and the lasing efficiency of PM567 in the solid matrix [47]. However, experimental results shown in figure 8 indicate that there is an optimal cross-linking degree that ameliorates the fluorescence and the lasing efficiencies. This optimal degree depends on the nature of the cross-linking agent. Thus, acrylic cross-linking agents (e.g. TMPTMA in scheme 3) optimize the fluorescence capacity and the lasing efficiency for a high proportion (around 10%, figure 8) of the cross-linking agent over the MMA monomers, while for the methacrylic agents (e.g. PETRA in scheme 3) low proportions of the cross-linking agents (around 1%, figure 8) are required to optimize the emission signals of PM567. This behaviour has been assigned to the different increases observed in the glass transition temperature ($T_g$) of the copolymer matrix, which is lower in the acrylic cross-linker than in the methacrylic agent, providing a less rigid environment in the former case [47]. A further increase in the cross-linking degree beyond this optimal point reduces the fluorescence capacity, probably because an excessively rigid environment damages the dye (figure 8). The experimental results shown in figure 8 support the adequate correlation between the fluorescence capacity and the lasing efficiency of alkyl-PM dyes, in the present case by changing the rigidity of the solid host polymeric material.

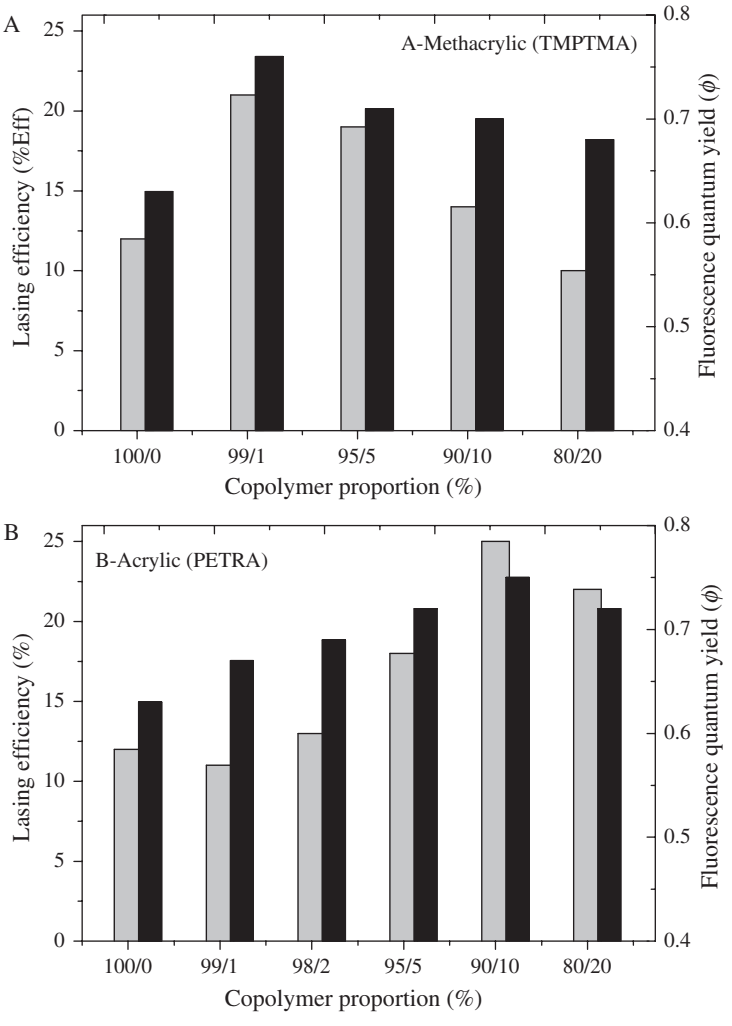


Figure 8. Evolution of the lasing efficiency [47] (grey) and the fluorescence quantum yield (black) with the methacrylic TMPTMA (A) and acrylic PETRA (B) cross-linking agent concentration.

### 3.4. *Acetoxy-pyrromethenes*

The photophysical properties of a series of new analogues of the PM567 dye with an acetoxy or a polymerizable acryloyl end group at the 8 position are studied in this section (scheme 2) [48, 49]. The acetoxy analogues are considered the molecular models for the derivatives with the polymerizable end group. Both end groups are separated from the chromophore by a linear polymethylene chain (PXAc or PXMA, linear analogues) with X = 1, 3, 5, 10 and 15 methylene units or by a *para* substituted phenyl group (PArXAc or PArXMA, phenyl analogues), or even double-substituted at the 2 and 6 positions (scheme 2). The study is performed in six representative solvents: apolar (*c*-hexane), polar (acetone and ethyl acetate) and polar/protic (ethanol,

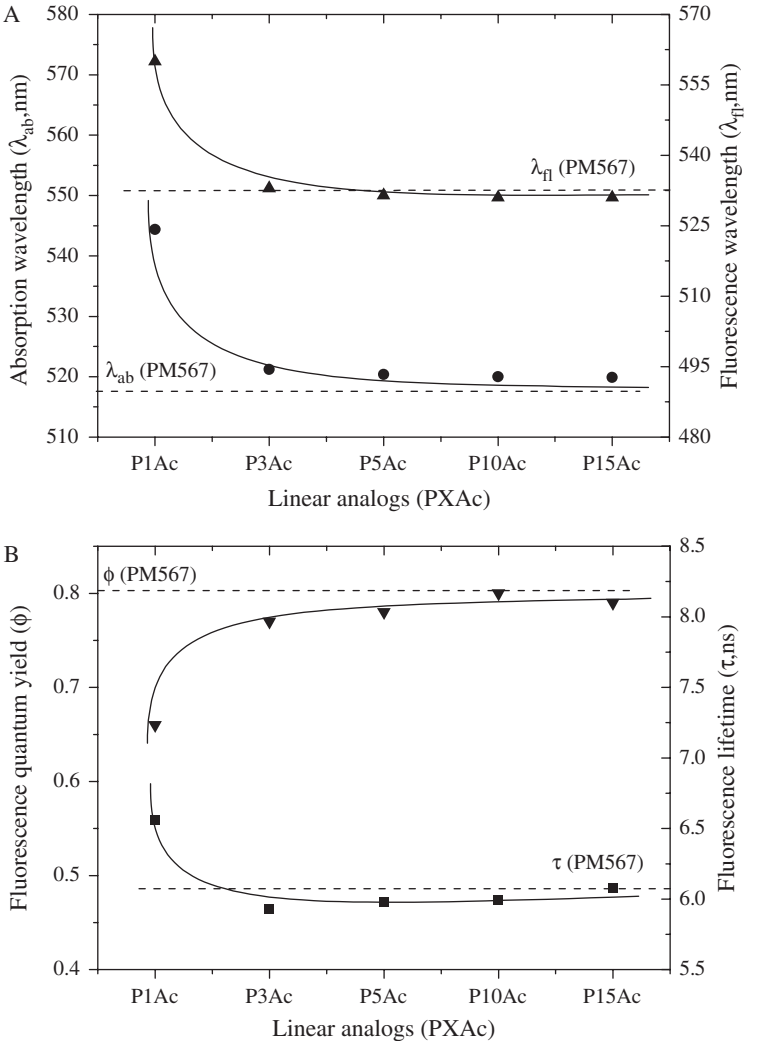


Figure 9. Evolution of the absorption ($\lambda_{ab}$, ●) and fluorescence ($\lambda_{fl}$, ▲) wavelength, and fluorescence quantum yield ($\phi$, ▼) and lifetime ($\tau$, ■) with the length of the chain of the linear PM567 analogues (PXAc, with X = 1, 3, 5, 10 and 15) in c-hexane. The corresponding values for the PM567 dye are shown as dashed lines.

methanol and trifluoroethanol) media and in solid polymeric matrices where the PM chromophore is incorporated to the polymer as a dopant or via a covalent linkage.

**3.4.1. Linear 8-acetoxy analogues.** The evolution of the photophysical properties of the linear acetoxy analogues with the length of the methylene linking chain is shown in figure 9. When the acetoxy group is close to the chromophore, i.e. only one methylene unit (X = 1), the photophysical properties of the chromophore drastically change

with respect to those of the original PM567 dye; spectral bands shift to lower energies, and the fluorescence capacity and lifetime decreases and increases, respectively, mainly due to a reduction in the $k_{fl}$ value. However, if the linking polymethylene chain length is long enough ($X \geq 3$ methylene units), the photophysical properties of these analogues tend to be those observed for PM567 (figure 9) [83]. Such behaviour is also predicted for the theoretical simulations of the absorption spectra [83]. These results rule out any direct intramolecular interaction between the acetoxy group and the electronic $\pi$-system of the chromophore. In fact, such an interaction should depend on the relative orientation of both groups and consequently would be favoured in long polymethylene chains where the flexibility and conformational distribution of the methylene units could place face-to-face both moieties. The optimized geometry (figure 10) of these PXAc analogues guarantees this argument, since it reveals a linear stair-like distribution of the methylene units in the linking chain where the end acetoxy group is placed far away from the aromatic ring. Therefore, the effect of the acetoxy group on the photophysics of the PM chromophore should be through the linking chain and it would be reduced by increasing the number of methylene units. Indeed, for $X \geq 3$ the effect of the acetoxy group on the photophysics of the chromophore is practically negligible (figure 9).

The influence of the acetoxy end group on the photophysics of the chromophore in the P1Ac can be explained by the contour maps of the frontier orbitals (figure 1). The electronic density at the 8 position is higher in the LUMO than in the HOMO orbital, hence an inductive electron withdrawing acetoxy group stabilizes more extensively the LUMO than the HOMO state, reducing the energy gap between the $S_0$ and $S_1$ states for the P1Ac dye. Moreover, such an electron acceptor acetoxy group would reduce the delocalization of the conjugated $\pi$-system, decreasing the $S_0$–$S_1$ transition probability for this derivative. For methylene linking chains of enough length (i.e. for more than three methylene units), the effects of the acetoxy group on the photophysics of PM dyes become nearly negligible. Consequently, linear methylene linking chains with more than three methylene units should be adequate candidates to incorporate



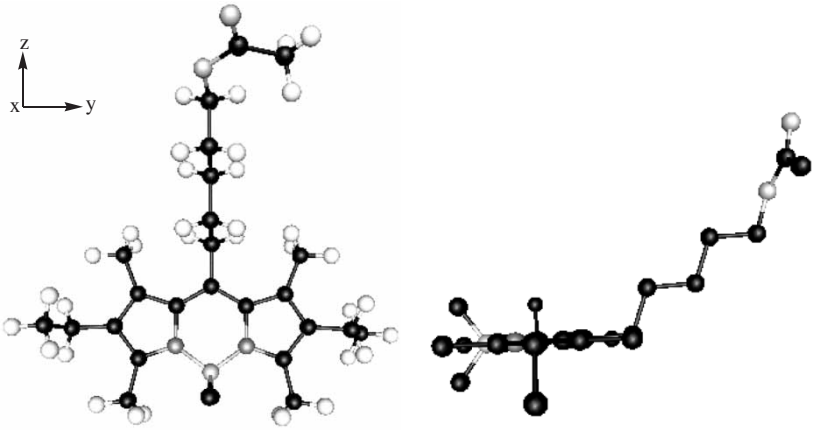


Figure 10. *x*- and *y*-perspectives of the optimized geometry of P5Ac analogue by the B3LYP/6-31G method.

polymerizable acryloyl end groups in order to covalently bind the PM chromophore in polymeric chains.

**3.4.2. 8-phenyl analogues.** The presence of the phenyl ring as a linking partner between the PM chromophore and the acetoxy end group does not drastically affect the photophysical properties of the PM567 dye (similar absorption and fluorescence wavelengths, and similar transition probabilities), although the presence of the phenyl group at the 8 position increases the radiationless deactivation processes (table 5) [72]. These results suggest the absence of any resonant interactions between the phenyl group and the chromophoric system. Indeed, this is corroborated by quantum mechanical calculations, since the phenyl group adopts a nearly perpendicular (dihedral angle 87.9°) [72] conformation with respect to the chromophoric ring in the optimized geometry of PAr1XAc analogues (figure 11). Such a conformation prevents any interaction between the electronic clouds of both systems. Other authors have claimed important changes in the photophysical properties of PM dyes by the presence of aromatic groups at the 8 position when there are no methyl groups at the adjacent 1 and 7 positions [35, 84, 85]. In that case, the coplanar disposition of both entities leads to a resonant interaction between the phenyl group and the chromophore extending the delocalization of the PM electronic $\pi$-system and giving rise to important changes in the photophysics of the PM chromophore [35]. This is not the present case and the nearly perpendicular disposition of both aromatic rings should be assigned to steric hindrances between the 1 and 7 methyl groups of the PM chromophore and the *ortho* hydrogens of the phenyl unit [72, 84]. Therefore, it could be concluded that the present aromatic phenyl group acts as a 'normal' linear linking polymethylene chain and the absorption and fluorescence bands of PArXAc are close to those of PXAc analogues with $X \geq 3$.

However, the aromatic analogues present an appreciable decrease in the $\phi$ and $\tau$ values with respect to those values of PM567, which are reflected in an increase in

Table 5. Photophysical properties of diluted solutions ($2 \times 10^{-6}$ M) of PAr1Ac and PAr3Ac dyes in six representative solvents.

| Solvent | $\lambda_{ab}$ (nm) | $\varepsilon_{max}$ ($10^4$ $M^{-1}cm^{-1}$) | $\lambda_{fl}$ (nm) | $\phi$ | $\tau$(ns) | $k_{fl}$ ($10^8$ $s^{-1}$) | $k_{nr}$ ($10^8$ $s^{-1}$) |
|---|---|---|---|---|---|---|---|
| *PAr1Ac* [49, 72] | | | | | | | |
| $F_3$-ethanol[a] | 521.6 | 6.56 | 535.2 | 0.81 | 6.35 | 1.27 | 0.30 |
| Methanol | 522.3 | 7.38 | 535.6 | 0.71 | 5.18 | 1.37 | 0.56 |
| Ethanol | 523.6 | 7.53 | 536.0 | 0.68 | 5.18 | 1.31 | 0.62 |
| Acetone | 522.2 | 7.02 | 536.0 | 0.65 | 4.82 | 1.34 | 0.73 |
| Ethyl acetate | 522.6 | 7.59 | 536.0 | 0.65 | 5.00 | 1.30 | 0.70 |
| *c*-hexane | 526.0 | 8.05 | 538.0 | 0.45 | 3.68 | 1.22 | 1.49 |
| *PAr3Ac* [49, 72] | | | | | | | |
| $F_3$-ethanol[a] | 520.2 | 6.90 | 534.0 | 0.90 | 6.51 | 1.38 | 0.15 |
| Methanol | 521.3 | 7.81 | 534.8 | 0.77 | 5.33 | 1.44 | 0.43 |
| Ethanol | 522.4 | 7.95 | 535.2 | 0.72 | 5.31 | 1.35 | 0.52 |
| Acetone | 521.4 | 7.91 | 535.2 | 0.65 | 4.92 | 1.32 | 0.71 |
| Ethyl acetate | 521.7 | 7.91 | 534.8 | 0.69 | 5.08 | 1.35 | 0.61 |
| *c*-hexane | 525.1 | 8.63 | 537.2 | 0.49 | 3.88 | 1.26 | 1.31 |

[a]2,2,2-trifluoroethanol.

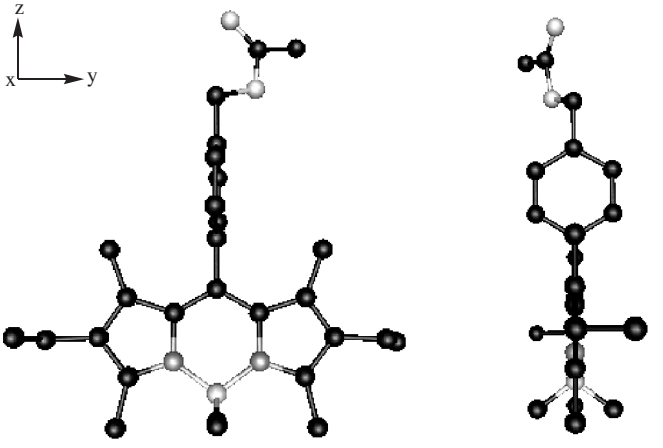


Figure 11. *x*- and *z*-views of the optimized geometries of PAr1Ac dye with B3LYP/6-31G.



the $k_{nr}$ value (table 5). Chen *et al*. [84] observed an important increase in $k_{nr}$ due to the presence of a phenyl unit and they attributed it to an augmentation in the internal conversion, which was assigned to the free rotation of the phenyl group with respect to the chromophoric ring. However, this mechanism is not valid in the present case, since the enhancement in the $k_{nr}$ value of PArXAc does not depend on the solvent viscosity when this parameter is included in the multilinear analysis (equation 6) of the solvent effect on the $k_{nr}$ value of these analogues [72]. Moreover, previous results on the photophysics of alkyl-PM dyes in benzene and toluene provided anomalously high values of $k_{nr}$ [45, 68]. Therefore, the increase in the radiationless deactivation of PArXAc could be assigned to internal conversion processes, probably due to a vibrational coupling between the PM and the phenyl ring, which can be performed via intramolecular (directly attached to the chromophore) and intermolecular (through the solvent) mechanisms [72].

On the other hand, the photophysical properties of the disubstituted analogue at the 2 and 6 positions (P3Ac2, scheme 2) are very close to those of the original dye PM567. The 2 and 6 positions of the chromophore are less sensitive to the substituent effect than the 8 position, since the change of the electronic density between the HOMO and LUMO states is higher at the latter position (figure 1).

Taking into account the lasing efficiencies of all these acetoxy PM567 analogues [49, 83], a satisfactory correlation between the lasing gain and the fluorescence quantum yield for both the substituent (phenyl group and the linear polymethylene chain) and the solvent effect is established, as shown in figure 12 for the former case. In fact, as can be seen from figure 12, the lowest laser efficiencies are obtained in the aromatic analogues (PAr1Ac and PAr3Ac) and in the linear-methylene P1Ac dye, while the lasing gain increases with the number of methylene units (PXAc with $X > 3$). The fluorescence capacity shows the same evolution explained above.

A new bichromophoric system based on the incorporation of a terphenyl group at the 8 position of the PM567 chromophore is now under study in our laboratory.

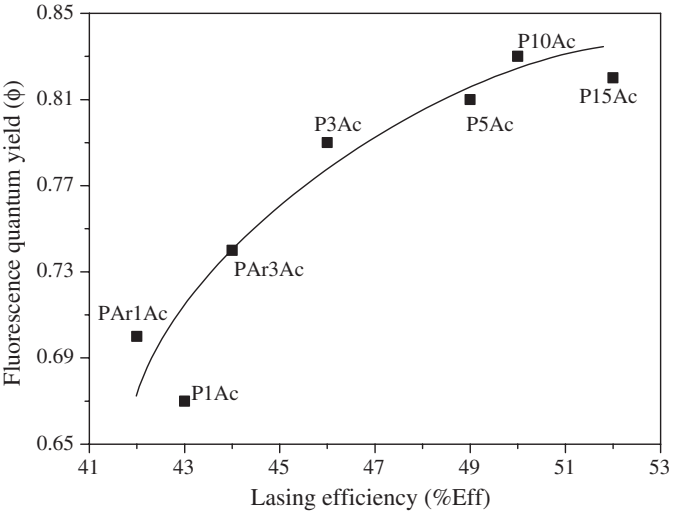


Figure 12. Correlation between the fluorescence quantum yield and the lasing efficiency [49, 83] of the linear (PXAc) and aromatic (PArXAc) analogues in polar media.



Preliminary results reveal that the excitation at the terphenyl absorption band ($\lambda_{ab} \approx 275$ nm) leads to its fluorescence emission ($\lambda_{fl} \approx 370$ nm) and also to the emission of the PM567 chromophore ($\lambda_{fl} \approx 530$ nm). Therefore, there is a partial energy transfer from the terphenyl excited state to the fluorescence state of the pyrromethene. This observation is of great technological interest in the development of new tunable laser systems based on the pumping of an adequate chromophore at a specific wavelength (e.g. in the UV region) and the laser emission of a second chromophore in the Vis region. Moreover, these energy-transfer systems are characterized by a high Stokes shift and would reduce the losses in the resonator cavity caused by the inner filter and reabsorption effects.

**3.4.3. Solid polymeric matrices.** The linear and aromatic acetoxy PXAc and PArXAc analogues have been incorporated [48, 49] in solid PMMA matrices as dopants (PXAc/PMMA), while the covalent linkage of the PM567 chromophore to the PMMA chain has been performed by the copolymerization of the corresponding PXMA analogues (with a polymerizable acryloyl end group) and MMA (the so-called COP(PXMA-MA), scheme 4) [82]. Besides, in the case of the disubstituted analogue, the PM567 chromophore is double-bounded to the polymeric chain and the dye itself can be considered to act as a cross-linker.

In general, the effect of the chain length or the phenyl group in the photophysical properties of the PM chromophore in polymeric hosts is similar to that described above in the liquid phase [72, 82, 83]. However, it has to be pointed out that the solid matrix yields slightly higher fluorescence capacities and lasing efficiencies for these PXAc and PXMA analogues with $X \geq 3$ methylene units than for the PM567 dye [45, 82]. These results corroborate the validity and the accuracy of the present

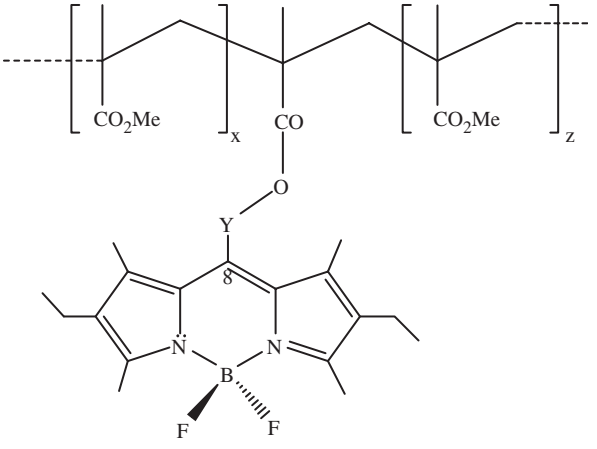


Scheme 4. Covalent linkage of the PM chromophore to a methacrylic chain.



Table 6. Photophysical and lasing [49, 82] properties of PM567 analogues (see scheme 2) incorporated as dopants (PXAc) and covalently linked to MMA (PXMA) through different spacers.

| | PXAc/PMMA [49, 82] | | | | | | PXMA-MMA [49, 82] | | | | | |
|---|---|---|---|---|---|---|---|---|---|---|---|---|
| X | $\lambda_{ab}$ | $\lambda_{fl}^{c}$ | $\lambda_{la}$ | $\phi^{c}$ | $\tau^{c}$ | %Eff | $\lambda_{ab}$ | $\lambda_{fl}^{c}$ | $\lambda_{la}$ | $\phi^{c}$ | $\tau^{c}$ | %Eff |
| *Linear* | | | | | | | | | | | | |
| 1 | 544.5 | 556.5 | 591 | 0.61 | 8.21 | 58 | 546.6 | 557.0 | 594 | 0.62 | 7.96 | 26 |
| 3 | 521.7 | 531.5 | 569 | 0.89 | 8.97 | 36 | 522.4 | 532.0 | 569 | 0.85 | 8.15 | 34 |
| 5 | 520.8 | 530.0 | 567 | 0.84 | 9.00 | 40 | 521.1 | 530.0 | 568 | 0.85 | 9.10 | 36 |
| 10 | 520.6 | 529.5 | 566 | 0.84 | 8.93 | 41 | 520.7 | 529.5 | 564 | 0.83 | 8.72 | 37 |
| 15 | 520.6 | 529.0 | 565 | 0.78 | 7.98 | 33 | 520.7 | 529.5 | 564 | 0.81 | 8.23 | 36 |
| 3-2 | 517.5 | 532.0 | 564 | 0.86 | 8.23 | 37 | 517.7 | 530.4 | 564 | 0.77 | 8.05 | 37 |
| *Aromatic* | | | | | | | | | | | | |
| Ar1 | 524.7 | 536.4 | 558 | 0.82 | 9.37 | 18 | 524.9 | 536.8 | 558 | 0.84 | 9.42 | 20 |
| Ar3 | 523.7 | 534.4 | 554 | 0.82 | 8.25 | 18 | 524.1 | 535.2 | 555 | 0.80 | 8.01 | 16 |

[c]Values corrected from the reabsorption and reemission phenomena [18].

linkage chain in the development of tunable lasers in the solid state based on these analogues. In general, the rigidity of the polymeric matrix favours the fluorescence capacity of these dyes.

Experimental results indicate that the photophysical properties of the acetoxy analogues included as dopants in the polymeric matrix are very similar to the corresponding acryloyl analogues covalently linked to the polymer chain (table 6) [82]. Therefore, the covalent linkage hardly affects the fluorescence capacity and the lasing efficiency of these dyes. However, it has been demonstrated that the covalent linkage considerably enhances the thermostability of the PM567 chromophore, probably because the chemical linkage provides extra pathways to the dye to eliminate the excess of heat accumulated during the laser action [82]. These results are of great importance in the application of PM dyes in tunable lasers, because the thermal degradation is one of the most important reasons for dye damage in solid state dye lasers. In this way,

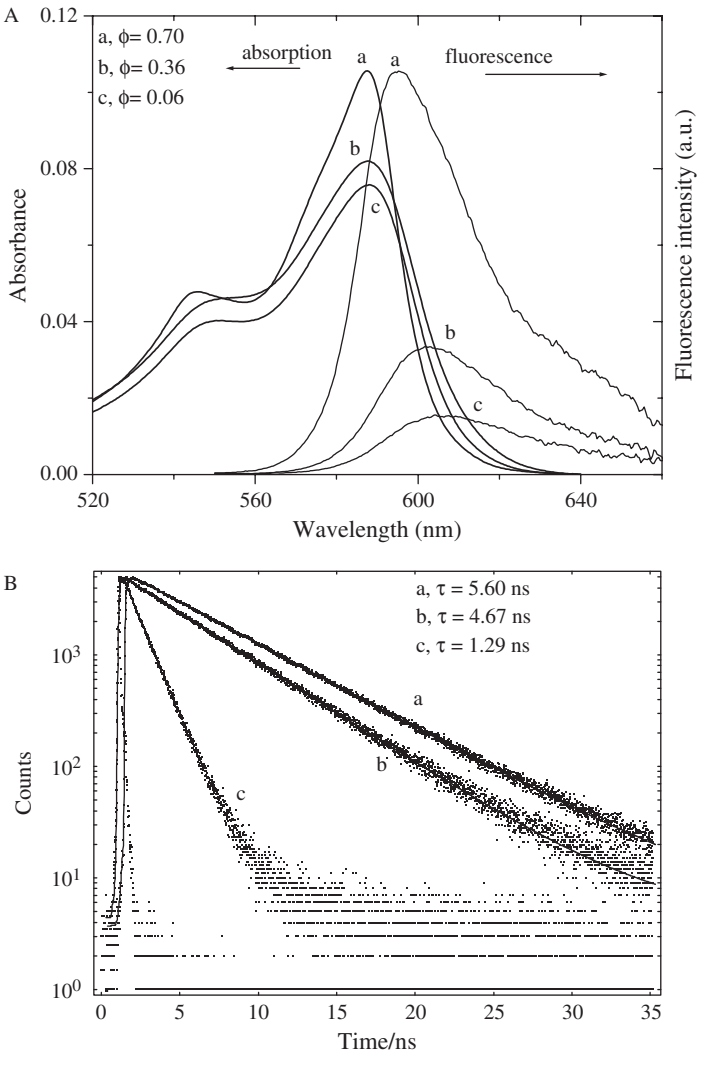


Figure 13. Absorption and fluorescence spectra (A) and fluorescence decay curves (B) of diluted solutions ($2 \times 10^{-6}$ M) of PM567 in *c*-hexane (a) and of PM650 in *c*-hexane (b) and methanol (c).

the operative lifetime of the active media is considerably increased by the covalent linkage [24].

### 3.5. *8-Cyano group: intramolecular charge transfer (ICT) state*

The PM650 dye presents a cyano group at the 8 position (scheme 1). Contrary to the preceding PM derivatives, PM650 presents drastic changes in the photophysical characteristics [86]. Figure 13 shows the important bathochromic shifts in both absorption and fluorescence bands of PM650 with respect to PM567. The presence of the cyano

Table 7. Photophysical properties of PM650 in diluted solutions ($2 \times 10^{-6}$ M) of *c*-hexane, acetone and methanol [86]. The theoretical results obtained by the semiempirical ZINDO and the *ab initio* TD-B3LYP methods are also included [86].

| | *c*-hexane | Acetone | Methanol | ZINDO | TD-B3LYP |
|---|---|---|---|---|---|
| $\lambda_{ab}$ (nm) | 589 | 588 | 588 | 523 | 473 |
| $\varepsilon$ ($10^4\,M^{-1}\,cm^{-1}$) | 5.30 | 3.45 | 4.10 | – | – |
| $f$ | 0.23 | 0.27 | 0.32 | 0.91 | 0.37 |
| $\lambda_{fl}$ (nm) | 600 | 606 | 609 | 525 | 475 |
| $\Delta\nu_{St}$ ($cm^{-1}$) | 290 | 510 | 610 | 70 | 90 |
| $\phi$ | 0.36 | 0.11 | 0.06 | – | – |
| $\tau$ (ns) | 4.67 | 1.81 | 1.29 | – | – |
| $k_{fl}$ ($10^8\,s^{-1}$) | 0.77 | 0.60 | 0.46 | 2.15 | 0.90 |
| $k_{nr}$ ($10^8\,s^{-1}$) | 1.37 | 4.92 | 7.29 | – | – |

group also significantly reduces the intensity of both bands, mainly in the fluorescence band in polar/protic solvents, due to a decrease in the transition probabilities and mainly to an increase in the non-radiative deactivation processes [87]. Table 7 summarizes the photophysical properties of PM650 in some representative solvents together with the theoretically predicted values. All these results indicate drastic effects on the photophysics of PM dyes due to the presence of a high electron acceptor substituent at the 8 position. The large bathochromic shift of both spectral bands with respect to those of the PM567 is assigned to a net stabilization of the LUMO level due to the cyano group decreasing the energy gap. Besides, this strong electron-withdrawing group reduces the delocalization of the chromophore leading to the observed decrease in the $k_{fl}$ value, which correlates with a diminution of the absorption intensity (table 7).

The presence of the cyano group also increases the $k_{nr}$ value, mainly in polar solvents (table 7). In order to carry out a deeper study of the solvent effect, the photophysical properties of the PM650 dye are registered in a multitude of apolar, non-basic polar and polar/protic solvents [86]. However, in the present case, the variety of solvents employed is limited, since we experimentally observed a degradation of PM650 and new absorption and fluorescence bands at higher energies in those polar media catalogued as electron donor solvents (e.g. amides). These solvents are not considered in the present paper because they have no interest from a photophysical point of view.

The multilinear analysis of the solvent effect on the photophysical properties of PM650 (figure 14) indicates an appreciable shift to lower energies of the fluorescence band with the solvent polarity, while the absorption band hardly shifts with the solvent. These results would indicate that the dipole moment of the chromophore practically does not change in the excitation process, but during the lifetime of the emissive excited state, there is a charge redistribution through the conjugated $\pi$-system increasing the dipole moment of the chromophore. Indeed, theoretical calculations at the DFT level suggest a low dipole moment of PM650 in the $S_0$ ground state ($\mu = 0.4$ D), much lower than that of PM546 ($\mu = 5.1$ D) [86]. The presence of an electron acceptor substituent at the 8 position of PM chromophores tends to change in the orientation of the dipole moment vector in the ground state, leading to a reduction in its value. However,

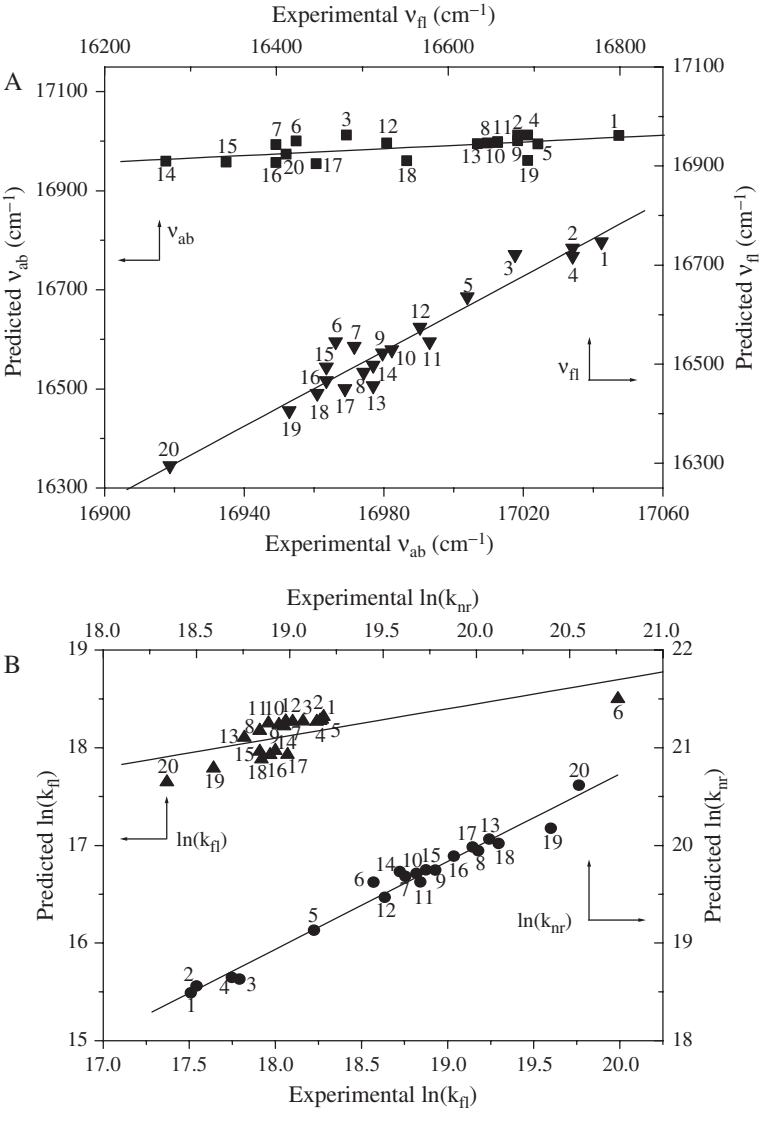


Figure 14. Correlation between the experimental (A) absorption ($\nu_{ab}$, ■) and fluorescence wavenumbers ($\nu_{fl}$, ▼) and (B) radiative ($k_{fl}$, ▲) and non-radiative ($k_{nr}$, •) deactivation rate constants with the corresponding predicted values by means of the Taft scales [76–78]. Apolar (1–4), polar/aprotic (5–13) and polar/protic (14–20) solvents [86].

because the electron transfer process is favoured in the excited states, the dipole moment of PM650 in the $S_1$ excited state ($\mu = 1.3$ D proposed by the *ab initio* CIS method) is higher than in the $S_0$ ground state. In this sense and contrary to the observation in alkyl-PM dyes, the excitation implies an augmentation in the dipole moment of the PM650 derivative [86].

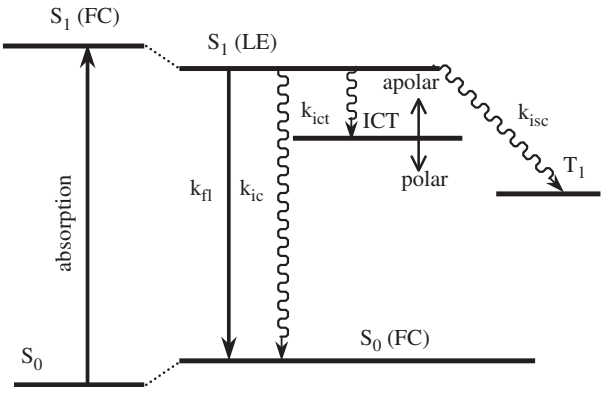


Figure 15. Energy diagram for the deactivation processes from the $S_1$ excited state of PM650: LE (Localize Excited), FC (Franck–Condon) and ICT (Intramolecular Charge Transfer) states. Continuous and wavy lines represent radiative and non-radiative processes, respectively. The stabilization of the ICT state with the solvent polarity is also illustrated.



Moreover, the multilinear regression analysis on the rate constant of the deactivation process shows that the $k_{fl}$ value slightly decreases and that the $k_{nr}$ value strongly increases with the solvent polarity/polarizability (figure 14). The previously described internal conversion mechanism related to the flexibility of the PM chromophore [72] is not applicable for the PM650 dye, since the optimized geometry by quantum mechanical calculation reveals a planar $\pi$-system. Therefore, a new mechanism for the radiationless deactivation in PM650, favoured in polar solvents, has been proposed. This extra non-radiative deactivation is assigned to the deactivation via an intramolecular charge transfer (ICT) state [88–91], obtained by electron transfer from the chromophoric $\pi$-system to the cyano group, as shown in figure 15. The ICT state is populated from the fluorescent $S_1$ local excited (LE) state and produces a quenching effect of its fluorescence emission [91]. The formation of the ICT state does not lead to new emission bands because the radiative deactivation is forbidden or because it deactivates to the $S_0$ ground state by a very fast non-radiative mechanism, preventing its further characterization by fluorescence techniques. The ICT state is characterized by a high dipole moment, and hence it is stabilized in polar media. Consequently, the fluorescent quenching of the LE emission is more efficient in polar solvents (figure 13 and table 7).

The drastic change in the fluorescence properties of PM650 depending on the nature of the solvent suggests the convenience of this PM derivative being used as a fluorescent molecular probe in the characterization of the physicochemical properties of different systems of special interest in biology, catalysis, etc. From a photophysical point of view, the cyano group would decrease the lasing efficiency of PM dyes. In this case, and contrary to the observation in alkyl and acetoxy PM dyes, apolar surroundings should be the recommended environments to achieve the highest laser efficiency. In fact, preliminary results obtained for the lasing characteristics [92] of the PM650 dye corroborate this suggestion; the lasing efficiency of PM650 is similar to that of

PM567 in *c*-hexane (with values around 30%) [92], whereas the former dye presents a much lower lasing efficiency in polar media (%Eff of around 15% for PM650 [92] vs. 55% for PM567 [45] in trifluoroethanol). The loss in the lasing efficiency of PM650 in polar solvents (around 4 times lower than that of PM567) is not so pronounced as the decrease in the fluorescence quantum yield (around 20 times), probably because the higher Stokes shift in PM650 reduces the losses by inner filter effects in the resonator cavity.

## 4. Conclusions

In general, the lasing characteristics of pyrromethenes dyes show an adequate correlation with their photophysical properties by changing the molecular structure of the dye and the nature of the solvent. Moreover, quantum mechanical calculations, at both the semiempirical and *ab initio* levels, can predict the effect of the substituent and the solvent on the photophysical characteristics of PM dyes. Therefore, quantum mechanical calculations are appropriate tools to orient the synthesis of new PM derivatives and to propose the best structural and environmental conditions to optimize the lasing properties of PM dyes.

Spectral band positions are better reproduced by semiempirical methods, although minor spectral shifts owing to the substituent and the solvent effects are more accurately predicted by DFT methods. Slight tuning in the spectral bands of PM dyes can be achieved by appropriate alkyl and polymethylene- or phenyl-acetoxy substituents at different positions of the chromophore. Non-radiative deactivation processes are favoured by bulky alkyl groups, probably due to a reduction in the planarity of the aromatic ring, and by phenyl groups, probably owing to a vibrational coupling between both aromatic systems. The presence of substituents with a high electron donor/acceptor capacity, such as a cyano group, leads to strong spectral shifts and diminution in the fluorescence capacity, due to a non-radiative deactivation process via non-fluorescence intramolecular charge transfer state. The important effect observed on the photophysics of this derivative by the solvent suggests the viability of PM650 as a fluorescent molecular probe, extending the applicability of the PM photophysics.

Polymethyl methacrylate matrices with appropriate rigidity are adequate host materials in the design of dye lasers in the solid state, since the polymeric systems do not extensively modify the photophysics of PM dyes. Moreover, the covalent linkage of the PM chromophore to polymeric chains, through methacryloyloxy substituents, improves the application of PM dyes as photonic materials, since the chemical bounding increases the thermo- and photostability of PM dyes.



## Acknowledgements

This work was supported by the Spanish MEC Minister (MAT2000-1361-C04-02) and the Basque Country University UPV/EHU (9/UPV00039.310-15264/2003). V.M.M. thanks the MECD Minister for a research grant.

## References


[1] F. P. Schafer, *Dye Lasers* (Springer-Verlag, Berlin, 1990).
[2] F. J. Duarte and L. W. Hillman, *Dye Lasers Principles* (Academic Press, New York, 1995).
[3] F. J. Duarte, *Tunable Lasers Handbook* (Academic Press, New York, 1995).
[4] F. J. Duarte, *Tunable Laser Optics* (Academic Press, San Diego, 2003).
[5] G. Calzaferri, S. Huber, S. Maas and C. Minkowski, Angew. Chem. Int. Ed. **42,** 3732 (2002).
[6] G. Schulz-Ekloff, D. Wöhrle, Van Duffel and R. A. Schoonheydt, Microporous Mesoporous Mater. **51,** 91 (2002) and references therein.
[7] N. Tyultyulkov, J. Fabian, A. Mehlhorn, F. Dietz and A. Tadjer, *Polymethine Dyes* (University Press, 1991).
[8] W. N. Sisk, K.-S Kang, M. Y. A. Raja and F. Farahi, Int. J. Optoelec. **10,** 95 (1995).
[9] S. Y. Lam and M. J. Damzen, Opt. Comm. **218,** 365 (2003).
[10] K. Rurack and U. Resch-Genger, Chem. Soc. Rev. **31,** 116 (2002).
[11] M. Maeda, *Laser Dyes* (Academic Press, Tokyo, 1984).
[12] J. Fabian and H. Hartmann, *Light Absorption of Organic Colorants* (Springer-Verlag, Berlin, 1980).
[13] L. J. Radziewski, R. W. Solarz and J. A. Paisner, *Laser Spectroscopy and its Applications* (Marcel Dekker, New York, 1987).
[14] F. J. Duarte, *Tunable Lasers Applications* (Academic Press, New York, 1995).
[15] T. G. Pavlopoulos, Prog. Quantum Elec. **26,** 193 (2002).
[16] F. López Arbeloa, P. Ruiz Ojeda and I. López Arbeloa, J. Chem. Soc. Faraday Trans. **2,** 1903 (1988).
[17] J. N. Demas and G. A. Crosby, J. Phys. Chem. **75,** 991 (1971).
[18] I. López Arbeloa, J. Photochem. **14,** 97 (1980).
[19] F. López Arbeloa, I. López Arbeloa and T. López Arbeloa, in *Handbook of Advanced Electronic and Photonic Materials and Devices*, edited by H.S. Nalwa (Academic Press, San Diego, 2001), Vol. 7, p. 209.
[20] M. D. Rahn and T. A. King, Appl. Opt. **34,** 8260 (1995).
[21] A. Costela, I. García-Moreno, J. M. Figuera, F. Amat-Guerri and R. Sastre, Laser Chem. **18,** 63 (1998).
[22] E. Yariv, S. Schulteiss, T. Saraidarov and R. Reisfeld, Opt. Mater. **16,** 29 (2001).
[23] A. Costela, I. García-Moreno and R. Sastre, in *Handbook of Advanced Electronic and Photonic Materials and Devices*, edited by H.S. Nalwa (Academic Press, San Diego 2001), Vol. 7, p. 161.
[24] A. Costela, I. García-Moreno and R. Sastre, Phys. Chem. Chem. Phys. **5,** 4745 (2003).
[25] S. Singh, V. R. Kanetkar, G. Sridhar, V. Muthuswamy and K. Raja, J. Luminiscence **101,** 285 (2003).
[26] R. Reisfeld, Opt. Mater. **16,** 1 (2001).
[27] M. Shah, K. Thangaraj, M.-L. Soong, L. T. Wolford, J. H. Boyer, I. R. Politzer and T. G. Pavlopoulos, Heteroatom Chem. **1,** 389 (1990).
[28] J. H. Boyer, A. M. Haag, G. Sathyamoorthi, M.-L. Soong, K. Thangaraj and T. G. Pavlopoulos, Heteroatom Chem. **4,** 39 (1993).
[29] T. G. Pavlopoulos, J. H. Boyer, M. Shah, K. Thangaraj and M.-L. Soong, Appl. Opt. **29,** 3885 (1990).
[30] J. H. Boyer, A. Haag, M.-L. Soong, K. Thangaraj and T. G. Pavlopoulos, Appl. Opt. **30**, 3788 (1991).
[31] S. C. Guggenheimer, J. H. Boyer, K. Thanagaraj, M. Shah, M.-L. Soong and T.G. Pavlopoulos, Appl. Opt. **32,** 3942 (1993).
[32] T. H. Allik, S. Chandra, T. R. Robinson, J. A. Hutchinson, G. Sathyamoorthi and J. H. Boyer, Mat. Res. Soc. Symp. Proc. **329,** 291 (1994).
[33] W. P. Partridge, N. M. Laurendeau, C. C. Johnson and R. N. Steppel, Opt. Lett. **19,** 1630 (1994).
[34] J. Karolin, L. B.-A. Johansson, L. Strandberg and T. Ny, J. Am. Chem. Soc. **16,** 7801 (1994).
[35] F. Li, S. I. Yang, T. Ciringh, J. Seth, C. H. Martin III, D. L. Singh, D. Kim, R. R. Birge, D. F. Bocian, D. Holten and J. S. Lindsey, J. Am. Chem. Soc. **120,** 10001 (1998).
[36] F. López Arbeloa, T. López Arbeloa and I. López Arbeloa, Recent Res. Devel. Photochem. Photobiol. **3,** 35 (1999).
[37] P. Toele, H. Zhang, C. Trieflinger and J. Daub, Chem. Phys. Lett. **268,** 66 (2003).
[38] M. O'Neal, Opt. Lett. **18,** 37 (1993).
[39] A. A. Gorman, I. Hamblett, T. A. King and M. D. Rahn, J. Photochem. Photobiol. A **130,** 127 (2000).
[40] M. D. Rahn, T. A. King, A. A. Gorman and I. Hamblett, Appl. Opt. **36,** 5862 (1997).
[41] M. S. Mackey and W. D. Sisk, Dyes and Pigments **51,** 79 (2001).
[42] M. Ahmad, T. A. King, D.-Y. Ko, B. H. Cha and J. Lee, Opt. Comm. **203,** 327 (2002).
[43] G. Jones II, Z. Huang and D. Pacheco, Proc. SPIE-Int. Soc. Opt. Eng. **4968,** 24 (2003).
[44] S. Y. Lam and M. J. Damzen, Appl. Phys. B **77,** 577 (2003).

[45] F. López Arbeloa, T. López Arbeloa, I. López Arbeloa, I. García-Moreno, A. Costela, R. Sastre and F. Amat-Guerri, Chem. Phys. **236,** 331 (1998).
[46] T. López Arbeloa, F. López Arbeloa, I. López Arbeloa, I. García-Moreno, A. Costela, R. Sastre and F. Amat-Guerri, Chem. Phys. Lett. **299,** 315 (1999).
[47] A. Costela, I. García-Moreno, C. Gómez, O. García and R. Sastre, J. Appl. Phys. **90,** 3159 (2001).
[48] F. Amat-Guerri, M. Liras, M. L. Carrascoso and R. Sastre, Photochem. Photobiol. **77,** 577 (2003).
[49] I. García-Moreno, A. Costela, L. Campo, R. Sastre, F. Amat-Guerri, M. Liras, F. López Arbeloa, J. Bañuelos Prieto and I. López Arbeloa, J. Phys. Chem. A **108,** 3315 (2004).
[50] T. López Arbeloa, F. López Arbeloa, P. Hernandez Bartolomé and I. Lopez Arbeloa, Chem. Phys. **160,** 123 (1992).
[51] A. Costela, I. García-Moreno, R. Sastre, F. López Arbeloa, T. López Arbeloa and I. López Arbeloa, Appl. Phys. B **73,** 19 (2001).
[52] W. Kohn, A. D. Becke and R. G. Parr, J. Phys. Chem. **100,** 12974 (1996).
[53] M. J. Frisch, G. W. Trucks, H. B. Schlegel, G. E. Scuseria, M. A. Robb, *et al. Gaussian-03* (Gaussian Inc., Pittsburgh PA, 2003).
[54] C. Lee, W. Yang and R. G. Parr, Phys. Rev. B **37,** 785 (1988).
[55] A. D. Becke, J. Chem. Phys. **104,** 1040 (1996).
[56] M. J. S. Dewar, E. G. Zoebisch, E. F. Healy and J. J .P. Stewart, J. Am. Chem. Soc. **107,** 3902 (1985).
[57] J. J. P. Stewart, *Mopac 2002* (Fujitsu Limited, Tokyo, 2001).
[58] J. B. Foresman, M. Head-Gordon, J. A. Pople and M. J. Frisch, J. Phys. Chem. **96,** 135 (1992).
[59] K. B. Wiberg, R. E. Stratmann and M. J. Frisch, J. Chem. Phys. **297,** 60 (1998).
[60] M. A. Thompson and M. C. Zerner, J. Am. Chem. Soc. **113,** 8210 (1991).
[61] A. Klamt, J. Phys. Chem. **99,** 2224 (1995).
[62] J. Tomasi and M. Persico, Chem. Rev. **94,** 2027 (1994).
[63] C. L. Picou, E. D. Stevens, M. Shah and J. H. Boyer, Acta Cryst. **C46,** 1148 (1990).
[64] J. Bañuelos Prieto, F. López Arbeloa, V. Martínez Martínez, I. López Arbeloa, Chem. Phys. **296,** 13 (2004).
[65] G. Bourhill, J.-L. Brédas, L.-T. Cheng, S. R. Marder, F. Meyers, J. W. Perry and B. G. Tiemann, J. Am. Chem. Soc. **116,** 2619 (1994).
[66] F. Bergström, I. Mykhalyov, P. Hägglof, R. Wortmann, T. Ny and L. B. A. Johansson, J. Am. Chem. Soc. **124,** 196 (2002).
[67] P. Acebal, S. Blaya and L. Carretero, Chem. Phys. Lett. **374,** 206 (2003).
[68] F. López Arbeloa, T. López Arbeloa and I. López Arbeloa, J. Photochem. Photobiol. A **121,** 177 (1999).
[69] T. López Arbeloa, F. López Arbeloa and I. López Arbeloa, Phys. Chem. Chem. Phys. **1,** 791 (1999).
[70] J. Bañuelos Prieto, F. López Arbeloa, V. Martínez Martínez, T. Arbeloa López and I. López Arbeloa, J. Phys. Chem. A **108,** 5503 (2004).
[71] E. Yariv and R. Reisfeld, Opt. Mater. **13,** 49 (1999).
[72] J. Bañuelos Prieto, F. López Arbeloa, V. Martínez Martínez, T. Arbeloa López, F. Amat-Guerri, M. Liras and I. Arbeloa López, Chem. Phys. Lett. **385,** 29 (2004).
[73] J. Bañuelos Prieto, F. López Arbeloa, V. Martínez Martínez, T. Arbeloa López and I. López Arbeloa, Phys. Chem. Chem. Phys. **6,** 4247 (2004).
[74] C. Reichardt, Chem. Rev. **94,** 2319 (1994).
[75] A. R. Katritzky, D. C. Fara, H. Yang, K. Tamm, T. Tamm and M. Karelson, Chem. Rev. **104,** 175 (2004).
[76] M. J. Kamlet and R. W. Taft, J. Am. Chem. Soc. **98,** 377 (1976).
[77] M. J. Kamlet and R. W. Taft, J. Am. Chem. Soc. **98,** 2886 (1976).
[78] M. J. Kamlet, J. L. M. Abboud and R. W. Taft, J. Am. Chem. Soc. **99,** 6027 (1977).
[79] J. Catalán, V. López and P. Pérez, J. Fluor. **6,** 15 (1996).
[80] J. Catalán, J. Palomar, C. Díaz and J. L. de Paz, J Phys. Chem. **101,** 5183 (1996).
[81] J. Catalán and C. Díaz, Liebigs Ann. Rec. 1941 (1997).
[82] F. López Arbeloa, J. Bañuelos Prieto, I. López Arbeloa, A. Costela, I. García-Moreno, C. Gómez, F. Amat-Guerri, M. Liras and R. Sastre, Photochem. Photobiol. **78,** 30 (2003).
[83] A. Costela, I. García-Moreno, C. Gómez, R. Sastre, F. Amat-Guerri, M. Liras, F. López Arbeloa, J. Bañuelos Prieto and I. López Arbeloa, J. Phys. Chem. A **106,** 7736 (2002).
[84] J. Chen, A. Burghart, A. Derecskei-Kovacs and K. Burguess, J. Org. Chem. **65,** 2900 (2000).
[85] A. Burghart, H. Kim, M. B. Welch, L. H. Thoresen, J. Reibenspies and K. Burgess, J. Org. Chem. **64,** 7813 (1999).
[86] F. López Arbeloa, J. Bañuelos Prieto, V. Martínez Martínez, T. Arbeloa López and I. López Arbeloa, Chem. Phys. Chem. **5,** 1762 (2004).

[87] G. Jones II, S. Kumar, O. Klueva and D. Pacheco, J. Phys. Chem. A **107,** 8429 (2003).
[88] A. Onkelinx, F. C. De Schryver, L. Viaene, M. Van der Auweraer, K. Iwai, M. Yamamoto, M. Ichikawa, H. Masuhara, M. Maus and W. Rettig, J. Am. Chem. Soc. **118,** 2892 (1996).
[89] K. Rurack, M. Kollmannsberger, U. Resch-Genger and J. Daub, J. Am. Chem. Soc. **122,** 968 (2000).
[90] M. Kollmannsberger, K. Rurack, U. Resch-Genger, W. Rettig and J. Daub, Chem. Phys. Lett. **329,** 363 (2000).
[91] N. Chattopadhyay, C. Serpa, M. M. Pereira, J. Seixas de Melo, L. G. Arnaut and S. J. Formosinho, J. Phys. Chem. A. **105,** 10025 (2001).
[92] A. Costela and I. García-Moreno, private communication.